The Astronomical Journal, 136:1587–1606, 2008 October doi:10.1088/0004-6256/136/4/1587

HOST GALAXIES OF LUMINOUS QUASARS: STRUCTURAL PROPERTIES AND THE FUNDAMENTAL PLANE

Marsha J. Wolf and Andrew I. Sheinis
Department of Astronomy, University of Wisconsin-Madison, 475 N. Charter Street, Madison, WI 53706, USA; mwolf@astro.wisc.edu, sheinis@astro.wisc.edu
Received 2007 October 18; accepted 2008 August 3; published 2008 September 10

ABSTRACT

We present stellar velocity dispersion measurements in the host galaxies of ten luminous quasars ($M_V < -23$) using the Ca H&K lines in off-nuclear spectra. We combine these data with effective radii and magnitudes from the literature to place the host galaxies on the fundamental plane (FP) where their properties are compared with other types of galaxies. We find that the radio-loud (RL) QSO hosts have similar properties to massive elliptical galaxies, while the radio-quiet (RQ) hosts are more similar to intermediate-mass galaxies. The RL hosts lie at the upper extreme of the FP due to their large velocity dispersions ($\langle\sigma_*\rangle = 321$ km s^{-1}), low surface brightness ($\langle\mu_e(r)\rangle = 20.8$ mag arcsec^{-2}), and large effective radii ($\langle R_e\rangle = 11.4$ kpc), and have $\langle M_*\rangle = 1.5 \times 10^{12}\,M_\odot$ and $\langle$M/L$\rangle = 12.4$. In contrast, properties of the RQ hosts are $\langle\sigma_*\rangle = 241$ km s^{-1}, $\langle M_*\rangle = 4.4 \times 10^{11}\,M_\odot$, and $M/L \sim 5.3$. The distinction between these galaxies occurs at $\sigma_* \sim 300$ km s^{-1}, $R_e \sim 6$ kpc, and corresponding $M_* \sim 5.9 \pm 3.5 \times 10^{11}\,M_\odot$. Our data support previous results that Palomar-Green QSOs are related to gas-rich galaxy mergers that form intermediate-mass galaxies, while RL QSOs reside in massive early-type galaxies, most of which also show signs of recent mergers or interactions. Previous authors have drawn these conclusions by using estimates of the black hole mass and inferring host galaxy properties from that, while here we have relied purely on directly measured host galaxy properties.

Key words: galaxies: active – galaxies: evolution – galaxies: formation – galaxies: fundamental parameters – galaxies: kinematics and dynamics – quasars: general

Online-only material: color figures

1. INTRODUCTION

A growing understanding of the connection between galaxies and their central black holes has emerged over the last decade. We now know that all galaxies with a bulge contain supermassive black holes (Kormendy 2004) and that black hole mass is correlated with host galaxy stellar velocity dispersion (Gebhardt et al. 2000a; Ferrarese & Merritt 2000; Tremaine et al. 2002). Furthermore, the inclusion of an amount of energy equal to that expected from active galactic nucleus (AGN) feedback to quench star formation above a critical halo mass in semianalytical galaxy formation models (Cattaneo et al. 2006; Dekel & Birnboim 2006) reproduces the galaxy demographics and bimodality of properties observed in large surveys (Sloan Digital Sky Survey (SDSS): Kauffmann et al. 2003a, 2003b; Hogg et al. 2003; Baldry et al. 2004; Heavens et al. 2004; Cid Fernandes et al. 2005; GOODS: Giavalisco et al. 2004; COMBO-17: Bell et al. 2004; DEEP/DEEP2: Koo 2003; Koo et al. 2005; Faber et al. 2007; MUNICS: Drory et al. 2001; FIRES: Labbé et al. 2003; K20: Cimatti et al. 2002; GDDS: McCarthy et al. 2004). These facts suggest that the growth mechanisms of the black hole and galaxy must be connected. However, details of the physical processes that make this connection, such as how AGN energy interacts with and is dissipated by surrounding halo gas, are not yet understood.

One way to investigate these processes is to understand the nature of the host galaxies. Does something in the galaxy trigger AGN activity? Do active quasars exist in galaxies with similar properties? Studies of AGN host galaxies have reached different conclusions. One group of collaborators (McLure et al. 1999; Hughes et al. 2000; Nolan et al. 2001) believes these objects are predominantly normal massive ellipticals. Nolan et al. found that most quasar host galaxies had evolved stellar populations that were 10 Gyr old with only a very small amount of recent star formation. However, in the first spectroscopic investigation of a sample of these objects, Miller (1981) concluded that they are not normal luminous ellipticals, a result that was later confirmed with deeper spectroscopy from the Keck telescope (Miller et al. 1996; Sheinis 2001; Miller & Sheinis 2003). Moreover, Canalizo & Stockton (2000, 2001) have seen evidence of star formation within the past 100 Myr in quasar hosts with far-infrared excesses using deep spectra from Keck. There is still debate about whether the different results are due to better quality spectra taken closer to the nucleus using 8–10 m class telescopes, or whether real differences exist in the host galaxy properties of the different quasar samples studied (Lacy 2006). This question will no doubt be answered as more data are analyzed from the larger extragalactic surveys.

In this work, we study luminous quasars ($M_V < -23$) in which the galaxy is actively feeding the central supermassive black hole. It is here that we should be able to investigate connections between the black hole and its surrounding galaxy from which we can draw conclusions about how the black hole may or may not affect galaxy formation and evolution. We begin in this first paper by analyzing the structural properties of the QSO host galaxies with the use of directly measured stellar velocity dispersions, which were previously unobtainable for quasars this luminous. We use these data to place the host galaxies on the fundamental plane (FP) and ascertain their structural properties relative to other types of galaxies. In future papers we will investigate whether these objects follow the $M_{\rm BH}$–σ relation and analyze the host galaxy stellar populations to look for indications of star-formation activity relative to quasar activity.

This paper is organized in the following manner. In Section 2 we describe the sample selection and data analysis including

our removal of scattered quasar light from the observed spectra and the measurement of stellar velocity dispersions. We also present the comparison objects from the literature that are used in our analysis. In Section 3 we use the fundamental parameters derived in Section 2 to analyze the FP locations and mass-to-light ratios of these objects. In Section 4 we discuss the properties of our QSO host galaxies relative to the comparison objects and their implication that two different classes of objects are present in our sample. Finally, in Section 5 we summarize our work and present the main conclusions. Further details about our stellar velocity dispersion measurement limitations and potential biases can be found in the Appendix.

2. DATA AND ANALYSIS

2.1. Sample Selection

Our full sample is primarily drawn from the 20 nearby luminous quasars of Bahcall et al. (1997), with the addition of a few objects from Dunlop et al. (2003) and Guyon et al. (2006). The analyses presented here include ten QSOs from this larger sample of 28 whose spectra show sufficient signal-to-noise ratio (S/N) to allow measurement of the velocity dispersion via the techniques described below. These ten objects are PG 0052+251, PHL 909, PKS 0736+017, 3C 273, PKS 1302-102, PG 1309+355, PG 1444+407, PKS 2135-147, 4C 31.63, and PKS 2349-014.

The full sample from Bahcall et al. (1997) was selected solely on the basis of luminosity ($M_V < -22.9$), redshift ($z \leqslant 0.20$), and galactic latitude ($|b| > 35^\circ$). All the quasars in the Véron-Cetty & Véron (1991) catalog that satisfied the redshift, luminosity, and galactic latitude criteria were included, amounting to 14 objects.

These 14 quasars with $z \leqslant 0.20$ have an average (median) absolute magnitude $\langle M_V \rangle = -23.4$ (23.2) and an average redshift $\langle z \rangle = 0.17$. Only three radio-loud (RL) quasars are present in the original sample of 14 objects. By combining the time available from GTO and GO programs, Bahcall et al. (1997) added an additional six quasars with redshifts in the range $0.20 < z < 0.30$; these additional objects satisfied the same luminosity and galactic latitude constraints as the original sample. The additional objects contained three RL quasars, bringing the total number of RL objects in the sample to 6 of 20 quasars.

Bahcall's final sample of 20 objects shows an average (median) absolute magnitude of −23.6 (−23.2) and an average redshift of $z = 0.19$. For nearly all (18) of the quasars, $15.1 < V < 16.7$, but two are much brighter in the optical band: 3C 273 ($V = 12.8$) and HE 1029–140 ($V = 13.9$).

2.2. Spectra

Off-nuclear spectra of seven of the host galaxies presented here were obtained with the Low Resolution Imaging Spectrograph (Oke et al. 1994) on the Keck telescope during 1996–1997. Typical offsets for the long-slit observations were 2–4″. Observed wavelength ranges covered ∼ 4500–7000 Å at a spectral resolution of $\Delta\lambda \sim 11$ Å (300 km s^{-1}). The average S/N Å^{-1} for the galaxies in this study ranges from 1.8 to 13.9, with a mean of 5.3, over the wavelength range of 3850–4200 Å. Further observation details for these Keck data can be found in Sheinis (2002) and Miller & Sheinis (2003).

We are currently obtaining spectra of additional host galaxies using an integral field unit (IFU), Sparsepak (Bershady et al. 2004, 2005), which feeds the Bench Spectrograph on the 3.5-m WIYN Telescope.[1] The central core of Sparsepak fibers are 4.″7 in diameter on 5.″6 spacings. Though not optimally sized for the host galaxies in this study that have typical effective radii of 1.3–6.″5, we are finding this IFU and the excellent image quality of WIYN to be quite effective in isolating host galaxy light from the central quasar light. We use a configuration of the Bench Spectrograph that provides an observed wavelength coverage of ∼4270–7130 Å at a resolution of $\Delta\lambda \sim 5$ Å (110 km s^{-1}). In the work presented here, PG 1309+355 was observed on WIYN in 2007 June; PHL 909 and PKS 0736+017 were observed in 2007 December. These spectra have S/N spanning of 2.4–8.9 Å^{-1}, with an average of 5.7 Å^{-1}, for exposure times of 2–4 hr.

2.3. Imaging

These objects all have *Hubble Space Telescope (HST)* or ground-based adaptive optics (AO) images in the archive for analysis of host galaxy properties. We take galaxy magnitudes and effective radii from the Bahcall et al. (1997) two-dimensional de Vaucouleurs profile fits for eight of the objects. These data for 4C 31.63 are provided by Hamilton et al. (2002) and Guyon et al. (2006) and for PKS 0736+017 by Dunlop et al. (2003). We use color corrections from Fukugita et al. (1995) and Poggianti (1997) to convert all to *r*-band and adopt a cosmology of $\Omega_M = 0.3$, $\Omega_\Lambda = 0.7$, and $H_0 = 70$ km s^{-1} Mpc^{-1}. Relevant object data are given in Table 1.

2.4. Comparison Galaxies

To aid in the interpretation of the nature of our QSO host galaxies, we will compare their structural properties to other types of galaxies. This comparison sample includes SDSS early-type galaxies from Bernardi et al. (2003a, 2003b, 2006). The Bernardi et al. (2003a) sample consists of nearly 9000 early-type galaxies that are placed on the FP in Bernardi et al. (2003b). Bernardi et al. (2006) search for the most massive galaxies by selecting SDSS objects with high stellar velocity dispersions, $\sigma_* > 350$ km s^{-1}, resulting in approximately 70 galaxies massive enough to be considered giant ellipticals. They find that these galaxies lie on the FP, but at its outer extreme.

For further comparison, we add the host galaxies of PG QSOs from Dasyra et al. (2007) who investigated the possibility that these QSOs were triggered during mergers of galaxies that contain gas, as are ultraluminous infrared galaxies (ULIRGs). They conclude that some, but not all, ULIRGs may undergo a QSO phase as the merger evolves and that the progenitors of both PG QSOs and ULIRGs are likely to be similar. Dasyra et al. (2007) compare their QSOs to a sample of galaxy merger remnants from Rothberg & Joseph (2006) that we add to our comparison as well. These objects were selected to be late-stage mergers in which the cores have coalesced into single nuclei.

The redshift distributions of our QSO host galaxies and the comparison samples are shown in Figure 1.

2.5. Surface Brightness and K-corrections

Host galaxy magnitudes in Bahcall et al. (1997) are given for the F606W *HST* filter. We convert these to *r*-band using their

[1] The WIYN Observatory is owned and operated by the WIYN Consortium, Inc., which consists of the University of Wisconsin, Indiana University, Yale University, and the National Optical Astronomy Observatory (NOAO). NOAO is operated for the National Science Foundation by the Association of Universities for Research in Astronomy (AURA), Inc.

Table 1
Object Data

#	Object Name	Redshift	B97 M_V(QSO)	H02 M_V(QSO)	B97 M_V(host)	H02 M_V(host)	M_V(host)[a]	F606-V	R_e	R_e	$\mu_e(r)$	Host	Radio
		(z)	(mag)	(mag)	(mag)	(mag)	(mag)	(mag)	(as)	(kpc)	(mag as^{-2})	Morphology	Loudness
(1)	(2)	(3)	(4)	(5)	(6)	(7)	(8)	(9)	(10)	(11)	(12)	(13)	(14)
1	PG 0052+251	0.1550	−24.1	−23.2	−22.5	−22.4	17.01	−0.31	1.8	4.8	19.36	Sb	RQ
2	PHL 909 *(0054+023)*	0.171	−24.1	−23.5	−22.2	−22.6	17.61	−0.41	2.3	6.7	20.43	E4	RQ
3	PKS 0736+017	0.191	...	−23.2	−22.6[b]	−22.8	17.51[b]	...	3.3	10.4[b]	21.01	E, int.	RL
4	3C 273 *(PG 1226+023)*	0.1583	−26.7	−26.7	−23.2	−23.6	16.40	−0.40	3.7	10.1	20.30	E4	RL
5	PKS 1302-102	0.2784	−25.9	−25.6	−22.9	−23.4	18.20	−0.50	1.4	5.9	19.56	E4(?)	RL
6	PG 1309+355	0.1840	−24.4	−24.1	−22.8	−23.1	17.15	−0.35	2.0	6.2	19.62	Sab	RQ
7	PG 1444+407	0.2673	−25.3	−24.9	−22.7	−23.3	18.27	−0.47	1.3	5.3	19.51	E1(?), S[e]	RQ
8	PKS 2135-147	0.2003	−24.7	−23.4	−22.4	−22.7	17.85	−0.45	2.6	8.6	20.83	E1	RL
9	4C 31.63 *(2201+315)*	0.2950	...	−25.1	...	−23.8	17.55[c]	...	6.5[d]	28.5	22.18	E[f]	RL
10	PKS 2349-014	0.1740	−24.5	−23.3	−23.2	−23.6	16.61	−0.41	4.8	14.2	21.02	E, int.	RL

Notes. Absolute magnitudes are calculated from apparent magnitudes with k-corrections. Column 2 is the object name, column 3 is the redshift, column 4 is the V-band absolute magnitude of the QSO from Bahcall et al. (1997), column 5 is the V-band absolute magnitude of the QSO from Hamilton et al. (2002), column 6 is the V-band absolute magnitude of the host galaxy from the best fit of Bahcall et al. (1997), column 7 is the V-band absolute magnitude of the host galaxy from the best fit of Hamilton et al. (2002), column 8 is the V-band apparent magnitude of the host galaxy from B97 $r^{1/4}$ 2D fits except as noted, column 9 is the F606W-V color from B97, column 10 is the effective radius in arcsec from B97 2D $r^{1/4}$ fits to F606W *HST* images, column 11 is the effective radius in kpc, column 12 is the r-band average surface brightness within R_e, column 13 is the host galaxy morphology from B97 except as otherwise noted, and column 14 is the radio loudness of the QSO: RL or RQ, divided at $L_{5\,\mathrm{GHz}} = 10^{26}$ W Hz^{-1} as in Kellermann et al. (1994).

[a] These magnitudes are from $r^{1/4}$ law fits, converted to the r-band using the average values of $B - V = 0.95$ and $B - r = 1.25$ from Faber et al. (1989) and Gebhardt et al. (2003). These values also correspond to the average of E and S0 galaxy color corrections from Fukugita et al. (1995).

[b] $M_{\mathrm{host}}(R)$ from Dunlop et al. (2003) and converted to M_V with color corrections from Fukugita et al. (1995), R_e from Dunlop et al. (2003).

[c] M_{host}(F702W) from Hamilton et al. (2002) converted to M_V with color corrections from Fukugita et al. (1995).

[d] Effective radius derived from 2D $r^{1/4}$ fit to the H-band AO image by Guyon et al. (2006).

[e] Morphology from Hamilton et al. (2002).

[f] Morphology from Hamilton et al. (2002) and Guyon et al. (2006).

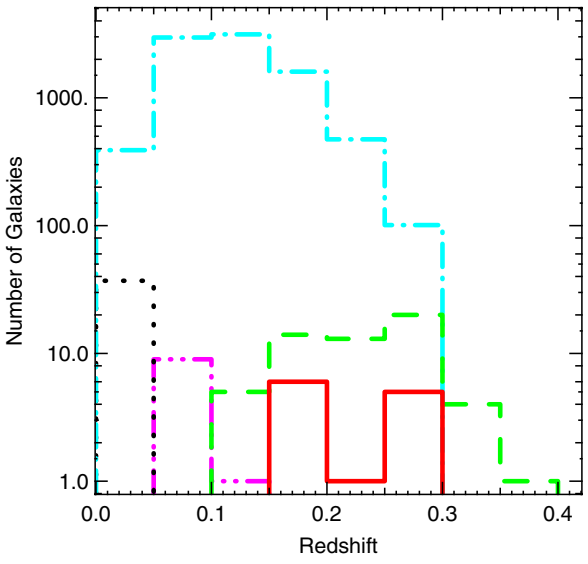

Figure 1. Redshift distributions of the galaxies. The solid red line is our sample of QSO host galaxies, the dot-dashed cyan line is the large sample of early-type SDSS galaxies (Bernardi et al. 2003a), the dashed green line is the sample of massive early-type SDSS galaxies with $\sigma_* > 350$ km s^{-1} (Bernardi et al. 2006), the dash-dotted-dot magenta line is the sample of PG QSO hosts (Dasyra et al. 2007), and the dotted black line is the sample of merger remnant galaxies (Rothberg & Joseph 2006).

(A color version of this figure is available in the online journal.)

F606-V colors for individual galaxies, and using the average colors for early-type galaxies from Faber et al. (1989) and Gebhardt et al. (2003), $B - V = 0.95$, and $B - r = 1.25$. We take the magnitudes of 4C 31.63 from Hamilton et al. (2002) in the F702W *HST* filter and of PKS 0736+017 from Dunlop et al. (2003) in the R-band, both of which we convert to r-band using average colors for E and S0 galaxies from Fukugita et al. (1995). With m_r we calculate host galaxy surface brightness from

$$\mu_e(r) = m_r + 2.5\log\left(2\pi R_e^2\right) - K(z) - 10\log(1+z), \quad (1)$$

as in Bernardi et al. (2003a), where R_e is in arcsec. K-corrections are given in Bernardi et al. (2003a) for the large sample of early-type galaxies and we use their values. To derive $K(z)$ for the other galaxies, we linearly fit the Bernardi et al. (2003a) K-corrections that are derived from a combination of Bruzual & Charlot (2003) models and early-type galaxy templates from Coleman et al. (1980), and apply them as $K(z) = 1.25z$ to the Bernardi et al. (2006) comparison galaxies and the QSO host galaxies (Figure 2). Below $z = 0.28$ this fit gives a median difference for the Bernardi et al. (2003a) galaxies of $\Delta K(z) = 0.0040$ with a standard deviation of $\sigma_{K(z)} = 0.0038$. Above $z = 0.28$, affecting 16 of the Bernardi et al. (2006) galaxies, these values change to $\Delta K(z) = -0.0080$ and $\sigma_{K(z)} = 0.0028$. Our $K(z)$ relation is extrapolated to redshifts higher than the fitted range for five of the Bernardi et al. (2006) galaxies.

2.6. Scattered QSO Light Removal

The light from the quasars in this study is as much as 3.5 mag brighter than the entire host galaxy. The regions of the host galaxies that we observed were typically 5–8 mag fainter than the quasar. As a result of the blurring produced by the Earth's

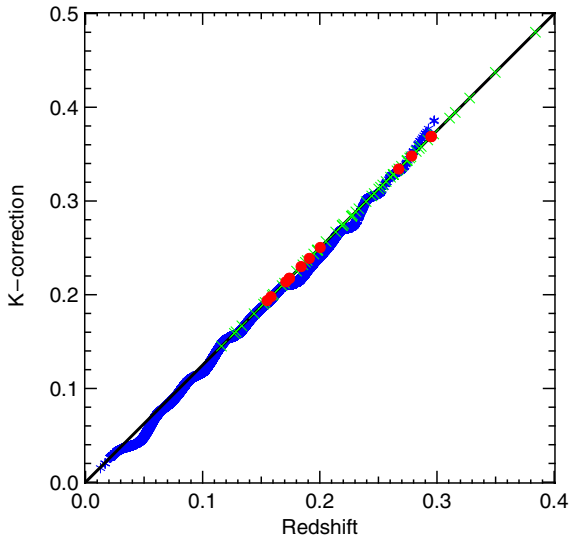

Figure 2. *K*-corrections for the *r*-band. The line is a linear fit to the *K*-corrections of the Bernardi et al. (2003a) galaxies (blue asterisks). This fit of slope 1.25 is applied to the redshifts of the Bernardi et al. (2006) galaxies (green crosses) and our QSO host galaxies (red circles) to derive their *K*-corrections.

(A color version of this figure is available in the online journal.)

atmosphere, plus a small contribution from the intrinsic optical point-spread function (PSF) and diffraction produced by the telescope, some light from the quasar entered the spectrograph in the off-nucleus observations, either long slit or fiber.

To spectrally remove the scattered light, we must both determine the fraction of light in the extracted spectrum that is from the quasar and also account for wavelength-dependent scattering efficiency due to atmospheric seeing (in the sense that as seeing gets worse, more scattering into a fixed offset distance from the quasar occurs with a shorter wavelength). We approximate these two factors by deriving a scattering efficiency curve of the form, $\psi = A_1 + A_2\lambda^{-A_3}$. We subtract the product of the scattering efficiency curve and the observed central quasar spectrum from the off-nuclear spectrum and iteratively fit that result by two-population stellar synthesis galaxy model spectra from Bruzual & Charlot (2003). Examples of this approach are shown for 4C 31.63 and PG 1444+407 in Figure 3, where the upper solid black lines are the observed off-nuclear spectra, the dotted blue lines are the product of the nuclear quasar spectrum and the derived scattering efficiency curve, and the lower solid red lines are the resulting scatter-subtracted host galaxy spectra. For this work we are concerned only with a small spectral region around the 4000 Å break to measure stellar velocity dispersion. This scatter-subtraction approximation is sufficient for such a small region. However, in future work, to accurately determine constituent stellar populations of the host galaxies using the entire observed spectrum, we plan to implement a more rigorous scattering model based on the geometry of the slit/fiber, its distance from the central quasar, approximate seeing conditions, and selective weighting of more important spectral features, such as QSO broad-line regions.

The basic model spectra fitting techniques used here are a modified version of Wolf et al. (2007) and Liu et al. (2007). We use six fitting parameters: old age, young age, luminosity-weighed fraction of the young age, and the scattering efficiency coefficients A_1, A_2, and A_3. Given the relatively low S/N of the spectra, we are not able to distinguish metallicity, so only [Fe/H] = 0 models are used. Age ranges for the old stellar population run from 10 Myr up to the age of the universe at the redshift of the quasar. Young ages are allowed to be any in the model grid that are younger than the current old age. χ^2 is calculated at each wavelength and weighted by the observed spectrum's noise at that point, $\chi_i^2 = \left[\left(F_{\mathrm{gal}_i} - \alpha F_{\mathrm{model}_i}\right)/\sigma_i\right]^2$, where F_{gal} is the flux of the scatter-subtracted galaxy spectrum, F_{model} is the flux of the model galaxy spectrum, α is a model spectrum normalization parameter, σ is the observed spectral noise, and the index i refers to each wavelength point. For the Keck data, noise spectra are generated by measuring the rms of the rest-frame spectrum at three locations devoid of prominent spectral features: ∼3600 Å, ∼5400 Å, and ∼6100 Å. We fit a polynomial to the measured rms values and extrapolate across the entire wavelength range to generate the galaxy's noise spectrum. For the WIYN data, noise spectra are calculated directly using the observed sky spectra. In both data, spectral features not included in the model spectra, such as sky residuals or galaxy emission lines, are masked and do not affect the χ^2 calculation. The best-fitting combination of parameters is selected as the one that provides the minimum χ^2 value when summed over wavelength.

2.7. Stellar Velocity Dispersions

We measure velocity dispersions from stellar absorption lines in the host galaxies by fitting a stellar template that has been convolved with a Gaussian profile to the off-nuclear, scatter-subtracted galaxy spectrum. The continuum is normalized on both galaxy and template spectra and a direct fit is done in pixel space using the code of Karl Gebhardt (Gebhardt et al. 2000b, 2003). The template is compiled from 21 weighted stellar spectra from the Coudé Feed Spectral Library at KPNO (Valdes et al. 2004), that were selected to provide a good representation of main sequence A stars through K giants. We use the same group of stars as Gebhardt et al. (2003), which are listed with their parameters in Table 2. We are able to use this library of stellar spectra taken with a different instrument because the spectral resolution ($\Delta\lambda = 1.8$ Å) is much higher than our host galaxy data. Fitting parameters include the weights of the individual stellar spectra and the Gaussian width to which the combined template is convolved. We select the best fit as the combination that provides the lowest rms differences from the galaxy spectrum.

Velocity dispersion uncertainties are calculated through Monte Carlo simulations by adding Gaussian noise to each pixel in the final template, which has a very high S/N, at a level such that the mean matches the noise in the initial galaxy spectrum and the standard deviation is given by the rms of the initial fit. The velocity dispersion is measured for 100 noise realizations and the mean and standard deviation of these results provide the measured velocity dispersion and its 1σ uncertainty. The distribution of measured values is also used to determine the sigma bias of the measurement. As long as the bias is much less than the uncertainty, the measurement is considered valid (see the Appendix).

We use the approximate wavelength range of 3850–4200 Å for our velocity dispersion fits, which contains the Ca II H&K (3968, 3934 Å) absorption lines. Even though these lines were historically avoided because of their intrinsic broadening, they have been shown to work very well in the presence of mixed stellar populations in galaxies (Kobulnicky & Gebhardt 2000; Gebhardt et al. 2003), as long as the mix of stellar spectra in the fitting template is individually determined for each galaxy. Greene & Ho (2006) also point out that the Ca H&K lines

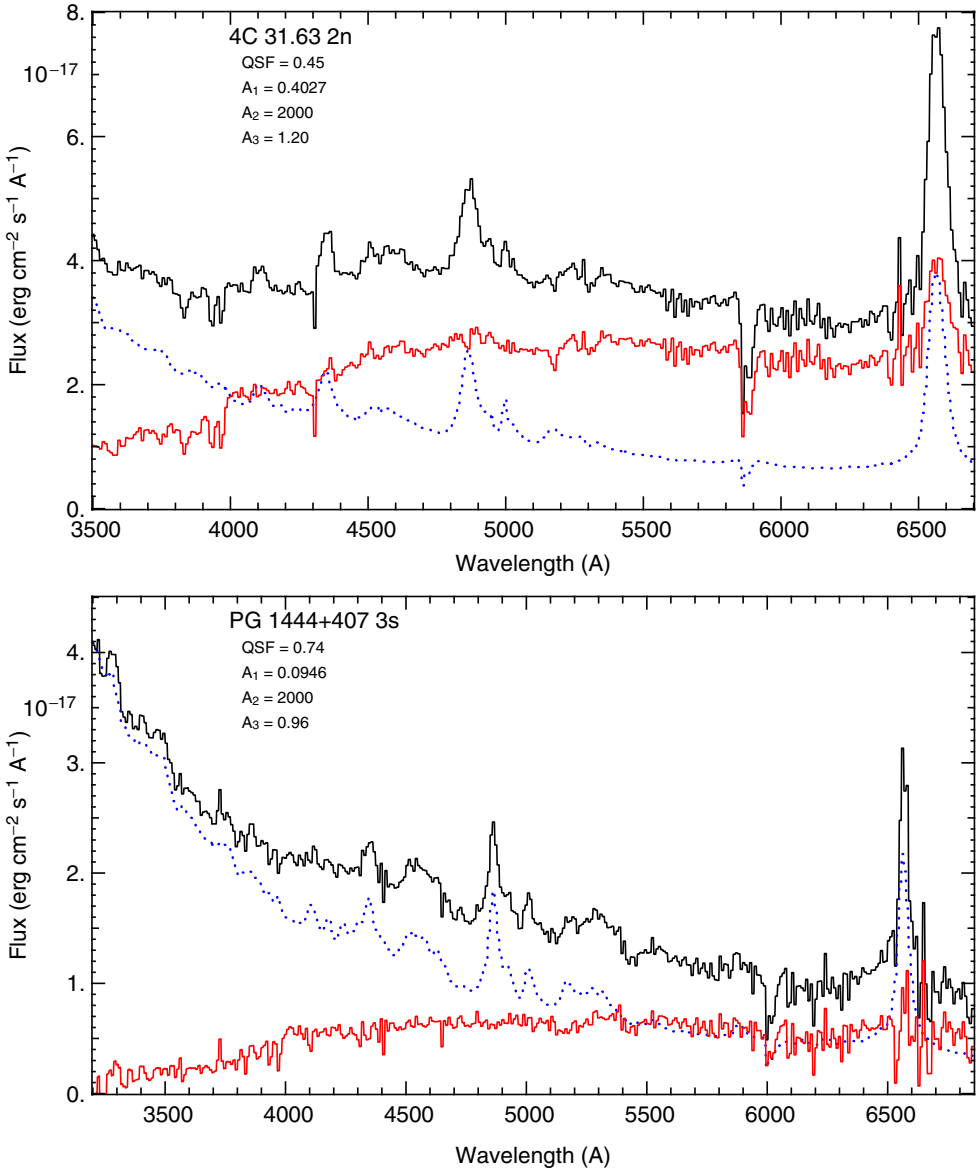

Figure 3. Examples of scattered quasar light removal on 4C 31.63 and PG 1444+407. The upper solid black lines are the extracted off-nuclear spectra, the dotted blue lines are the products of the scatter efficiency curves (with given best-fit parameters) and the nuclear quasar spectra, and the lower solid red lines are the final scatter subtracted host galaxies. All are binned to the instrumental resolution. QSF is the total quasar scattered light fraction in the extracted spectrum.

(A color version of this figure is available in the online journal.)

should be good for measuring σ_* in powerful AGNs because they may be the only stellar absorption lines with sufficient equivalent width to persist in high-luminosity AGNs. We mask a few features in the region including Hδ since Balmer line widths may be dominated by rotation and pressure broadening of A stars; the H8 line just blueward of Ca K; and the Ca H line in some cases that show contamination. We also tested the Mg I*b* triplet (5167, 5173, 5184 Å) region and found that it did not produce reliable results in these data (see the Appendix).

The velocity dispersion fits for our ten host galaxies are shown in Figure 4. The black solid lines are the galaxy spectra and the dashed red overlays are the best-fitting templates. The yellow shaded regions mark features that were masked and disregarded during the fit. PKS 2135-147 contained particularly strong broad QSO emission at the Ca H line. 3C 273 and PKS 2349-014 also show contamination from narrow emission near this line. Our measured dispersions are given in Table 3, along with the radii at which the galaxies were observed, the relative fractions of stars in the best-fitting template (A V, F-G V, G-K III), the spectral S/N over the fitted region, and the amount of scattered quasar light that was removed from the spectrum. The measured velocity dispersions range from 150 to 346 km s^{-1} with a mean of 272 km s^{-1}. We tested the possibility of the A stars in the template inflating the velocity dispersions measured from the Ca II lines by removing them from the available stellar templates and got the same results within the uncertainties. In fact, the measured σ's with the A stars in the mix were systematically lower by $\sim$7%.

Note that three velocity dispersions are marked as upper limits. Tests on velocity dispersion standard galaxies of McElroy (1995) show that we should be able to measure down to about 20% below the instrumental resolution of 300 km s^{-1}, or 240 km s^{-1} (see the Appendix). We mark any measurements $<$250 km s^{-1} as upper limits. For PG 0052+251, even though its fit looks reasonable in Figure 4, the measured σ_* exhibits higher sigma bias than the rest of our objects over the range of

Table 2
Stars Used in Template Spectra

Name (1)	Type (2)	$T_{\rm eff}$ (K) (3)	log g (4)	[Fe/H] (5)
HD 39283	A2V	4000	1.3	−0.12
HD 60179	A1V	10286	4	0.98
HD 85235	A3IV	11200	3.55	−0.4
HD 70110	F9V	5955	4.07	0.07
HD 10307	G1.5V	5898	4.31	−0.02
HD 199960	G1V	5813	4.2	0.11
HD 52711	G4V	5890	4.31	−0.16
HD 111812	G0IIIP	...	...	0.01
HD 161797	G5IV	5411	3.87	0.16
HD 107950	G6III	5030	2.61	−0.16
HD 10761	G8III	4980	2.82	−0.11
HD 181276	G9III	5000	2.95	−0.08
HD 219449	K0III	4575	2.1	−0.03
HD 220954	K1III	4625	1.95	−0.08
HD 76291	K1IV	4536	2.74	0.08
HD 81146	K2III	4370	2.34	0.01
HD 173780	K3III	4400	2.57	−0.12
HD 124547	K3III	4130	2.04	0.17
HD 136726	K4III	4120	2.03	0.07
HD 120933	K5III	3820	1.52	0.5
HD 112300	M3III	3700	1.3	−0.16

input σs relevant for our spectral resolution (see the Appendix). The data seem to indicate that the true σ_* is below our resolution. Therefore, we can only give an upper limit on the velocity dispersion of PG 0052+251. On close inspection of its spectrum, this measurement may be affected by insufficient scatter subtraction of an Ne III emission line at 3969 Å in the quasar spectrum (Hewitt & Burbidge 1993) that falls in the vicinity of the Ca H&K lines, causing a strange shape to the lines (Figure 4). Despite the fact that this galaxy has a relatively high S/N, the amount of scattered quasar light and location of this feature prevent accurate scatter subtraction around these lines. Figure 5 shows our scatter subtraction of PG 0052+251 with the Ca H&K lines marked and the stellar population model fit for this galaxy. Although the continuum and many other features of the host galaxy are fit very well by the model, the line depths between 3800 and 4100 Å, which is riddled with quasar emission, are very discrepant, signaling that the galaxy absorption lines may be contaminated. It is possible that this could contribute to the problematic sigma bias in the velocity dispersion measurements on this galaxy. A further discussion of tests of σ_* measurement on galaxy spectra diluted by residual scattered quasar light can be found in the Appendix.

2.7.1. Aperture Correction

Because velocity dispersion varies with galaxy radius, to match the comparison data we aperture-correct all host galaxy velocity dispersions from the radius at which σ_* was measured to the radius of $R_e/8$, as in Bernardi et al. (2003a) (see Jørgensen et al. 1995),

$$\sigma_{\rm cor} = \sigma_{\rm meas}\left(\frac{R_{\rm obs}}{R_e/8}\right)^{0.04}. \quad (2)$$

In the Keck data, the host galaxy spectra are off-nuclear long-slit observations for which the extracted spectra are summed along the slit; therefore, the weighted average radius along the summed portion of the slit is used as the effective observed radius. For the WIYN data, the approximate radius at which the fiber was centered is used. Effective observed radii are given in Table 3. Aperture-corrected velocity dispersions of the host galaxies are used in the following FP analysis. Average aperture corrections are 9% for these galaxies.

3. RESULTS

3.1. The Fundamental Plane

Previous work has shown that host galaxies of AGN lie on the FP occupied by quiescent early-type galaxies (e.g., Woo et al. 2004; Treu et al. 2007; Dasyra et al. 2007). Here we explore the properties of the host galaxies of higher-luminosity quasars. We place the QSO host galaxies on the FP in Figure 6, using the r-band projection against effective radius, R_e from Bernardi et al. (2006),

$$\log\sigma_* + 0.2\,[\mu_e(r) - 19.64]\,, \quad (3)$$

with R_e in kpc, the stellar velocity dispersion, σ_*, in km s^{-1}, and the surface brightness, μ_e(r), in mag arcsec^{-2}. Our QSO host galaxies are shown as large circles (green are RL and yellow

Table 3
Host Galaxy Velocity Dispersions

Object Number (1)	Object Name (2)	Measured σ_* (km s^{-1}) (3)	σ_* Error (km s^{-1}) (4)	$R_{\rm avg}$ (arcsec) (5)	$f_{\rm AV}$ (6)	f_{F-GV} (7)	f_{G-KIII} (8)	S/N Å^{-1} (3850–4200 Å) (9)	$f_{\rm QSO}$ (10)	Inst. Res. (km s^{-1}) (11)
1	PG 0052+251 3S	<250.0	52.9	3.63	0.46	0.00	0.54	13.9	0.67	300
2	PHL 909 4.5N	149.5	10.8	4.5	0.0	0.0	1.0	5.8	0.67	110
3	PKS 0736+017 4.5NW	311.0	82.9	4.5	0.0	0.0	1.0	2.4	0.46	110
4	3C 273 4N	305.3	57.5	4.36	0.18	0.82	0.00	4.5	0.40	300
5	PKS 1302-102 2.3N	346.3	72.4	3.05	0.07	0.93	0.00	2.2	0.78	300
6	PG 1309+355 4.5SW	235.9	29.8	4.5	0.06	0.09	0.85	8.9	0.39	110
7	PG 1444+407 3S	278.9	22.4	3.70	0.27	0.73	0.00	4.4	0.74	300
8	PKS 2135-147 3W	278.4	105.9	3.81	0.39	0.00	0.61	3.0	0.69	300
9a	4C 31.63 3S	<245.8	36.5	3.0	0.00	1.00	0.00	2.0	0.27	300
9b	4C 31.63 2N	289.9	22.7	2.0	0.06	0.94	0.00	5.6	0.45	300
9c	4C 31.63 2.5E	324.9	24.2	2.5	0.14	0.00	0.86	13.4	0.08	300
10a	PKS 2349-014 3S	<223.7	33.9	3.24	0.00	0.00	1.00	1.8	0.27	300
10b	PKS 2349-014 4N	278.3	54.0	4.83	0.00	0.00	1.00	2.0	0.30	300

Notes. The velocity dispersions listed here are not aperture corrected. Aperture corrections range from 6% to 13% with an average of 9%. Any measured σs less than 250 km s^{-1} are marked as upper limits. The measurement on PG 0052+251 has other problems described in the text.

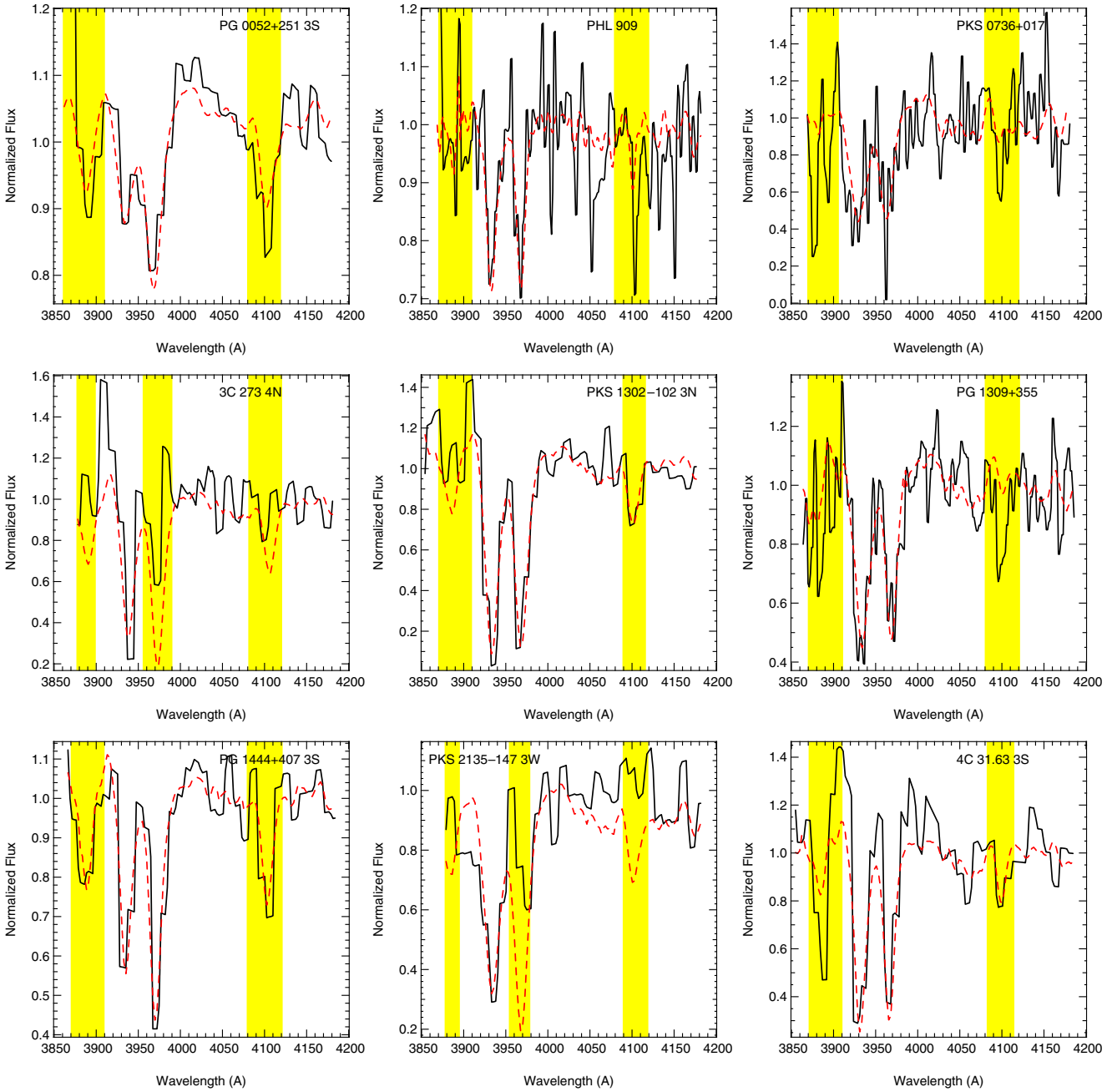

Figure 4. Velocity dispersion fits to the Ca H&K line region. The solid black lines are the host galaxy spectra, the dashed red lines are the combined stellar templates convolved with the best-fitting Gaussian line profiles, and the yellow shading marks regions that were masked during the fit.

(A color version of this figure is available in the online journal.)

are radio-quiet (RQ), using the division defined in Kellermann et al. 1994 at $L_{5\,\mathrm{GHz}} \sim 10^{26}$ W Hz^{-1}). The numbers inside these symbols correspond to object numbers in the tables. The PG QSO host galaxies of Dasyra et al. (2007) are shown as triangles. These objects are all RQ and some have known morphologies (Guyon et al. 2006): the large filled triangles are ellipticals, the crosses on triangles denote ellipticals with signs of interaction, the large open triangles are early types, the large open triangles with asterisks are spirals, and the small filled triangles are unknown. Comparison of SDSS early-type galaxies are the small cyan points (Bernardi et al. 2003a) and early types with $\sigma_* > 350$ km s^{-1} (Bernardi et al. 2006) are the open diamonds. Merger remnant galaxies from Rothberg & Joseph (2006) are denoted as squares: normal mergers are shown as filled red squares, luminous infrared galaxies (LIRG)/ULIRGs as filled black squares, and shell ellipticals as open squares.

The QSO hosts occupy both regions covered by the Bernardi et al. (2003a, 2006) early-type galaxy samples, while the merger remnants lie within or below the main early-type galaxy distribution. All of our RL QSO hosts lie near the upper envelope of the FP, while the RQ objects (both ours and those of Dasyra et al. 2007) mostly lie within the main locus. The implications of a location in the upper envelope of the FP are higher stellar velocity dispersion, lower surface brightness, or larger effective radius than normal for typical early-type galaxies. The Bernardi et al. (2006) galaxies occupy this region as well. Bernardi et al. concluded that these massive galaxies were not outliers, but merely at the outer extreme of the FP distribution. Figure 7 plots

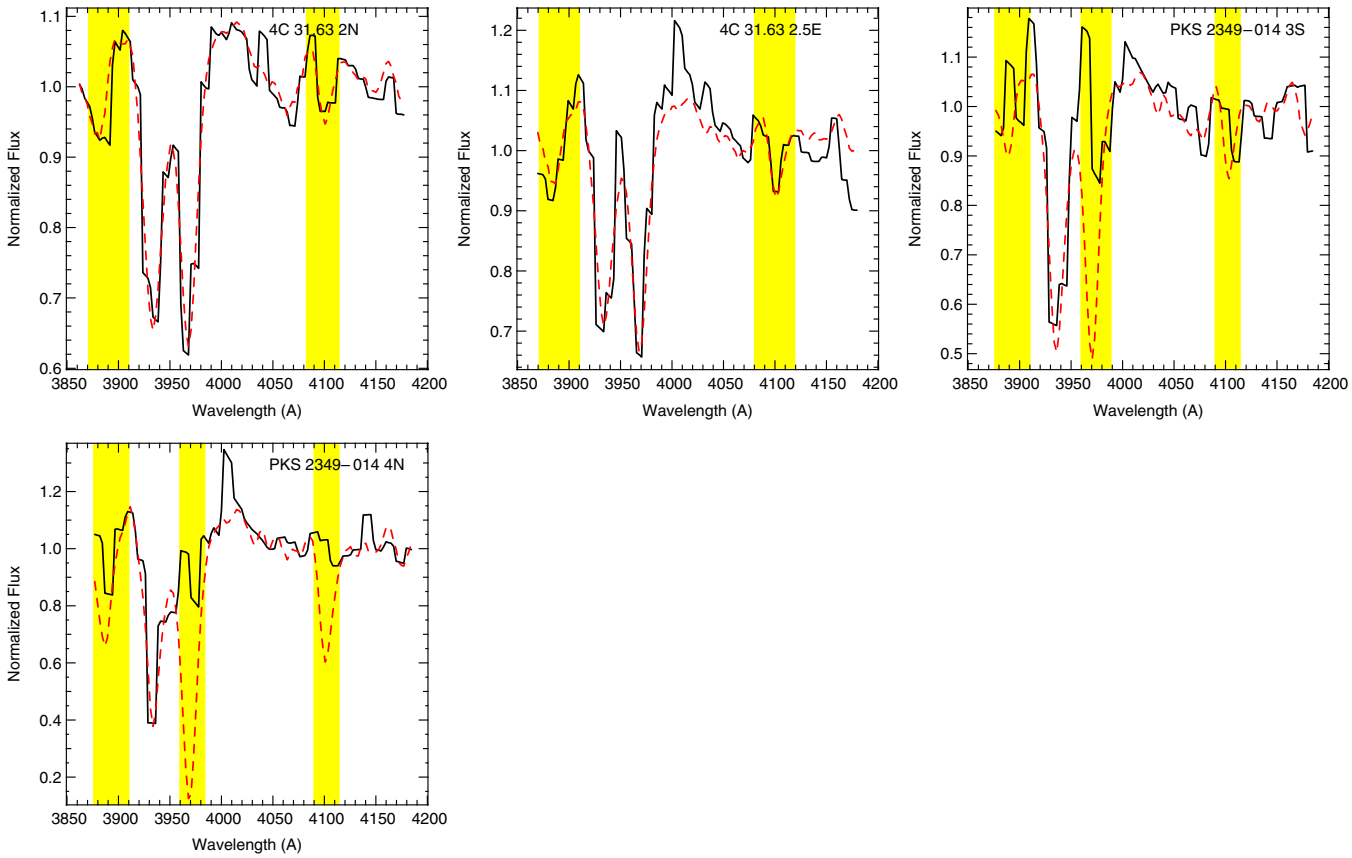

Figure 4. (Continued)

the fundamental galaxy parameters against each other. It is clear from these plots that our host galaxies at the upper extreme of the FP have systematically higher velocity dispersions, lower surface brightnesses, and larger effective radii than the normal early-type galaxies.

A caveat to keep in mind is that we have used surface brightnesses and effective radii derived from two-dimensional de Vaucouleurs profile fits to all galaxies, regardless of morphology. This was an attempt to analyze all objects in the same way for comparison; however, some objects have obvious morphological disturbances atypical of early-type galaxies. Three host galaxies of RQ QSOs show obvious spiral structure. The consequences of fitting disk galaxies with an $r^{1/4}$ model, which is more characteristic of their bulges, is discussed in Section 4.1.

3.2. Mass-to-Light Ratios

Now we explore the behavior of the mass-to-light ratios (M/L) of the galaxies. For this analysis we calculate the galaxy mass from

$$M_* = \frac{5\sigma_*^2 R_e}{G}[M_\odot], \quad (4)$$

where 5 is a structural constant corresponding to $R_{\rm tidal}/R_{\rm core} \approx 100$, where $R_{\rm core}$ is the radius at which surface brightness has dropped to half its central value, for King surface brightness models of giant to intermediate-mass ellipticals (Bender et al. 1992). The luminosity is calculated from

$$L = 2\pi \langle I_e \rangle R_e^2 [L_\odot], \quad (5)$$

with $\langle I_e \rangle$, the mean surface brightness within R_e, calculated from

$$\log\langle I_e \rangle = -0.4(\langle \mu_e \rangle - c_1 - c_2(z))[L_\odot {\rm pc}^{-2}], \quad (6)$$

Table 4
Host Galaxy M/L and Mass

Object Number (1)	Object Name (2)	M/L $(M_\odot/L_\odot)$ (3)	M_* $10^{11}M_\odot$ (4)
1	PG 0052+251	<5.6	<4.4
2	PHL 909	3.8	2.2
3	PKS 0736+017	17.8	14.1
4	3C 273	9.1	13.1
5	PKS 1302-102	10.3	10.3
6	PG 1309+355	5.0	5.0
7	PG 1444+407	7.2	6.2
8	PKS 2135-147	14.6	9.4
9	4C 31.63	14.3	30.1
10	PKS 2349-014	8.3	12.2

where $c_1 = 26.4$ for the Gunn r-band (Jørgensen et al. 1996), $c_2(z)$ is a redshift-dependent correction to our cosmology, and μ_e is the surface brightness in units of mag arcsec^{-2}.

Table 4 gives the values of M/L and stellar mass for our host galaxies and the lower-right panel of Figure 7 shows the calculated M/L as a function of velocity dispersion for our hosts and the comparison objects. As noted in Bernardi et al. (2003b), the slope of the (M/L)–σ_* relation can be quite different when the M/L calculated from observables is compared with that predicted from the FP. Therefore, we use the M/L calculated from observables. The host galaxies of RL quasars show a systematically higher M/L than that of the RQ objects.

3.3. Individual Objects

We now compile all information on our individual QSOs and their host galaxies. The magnitudes quoted in this

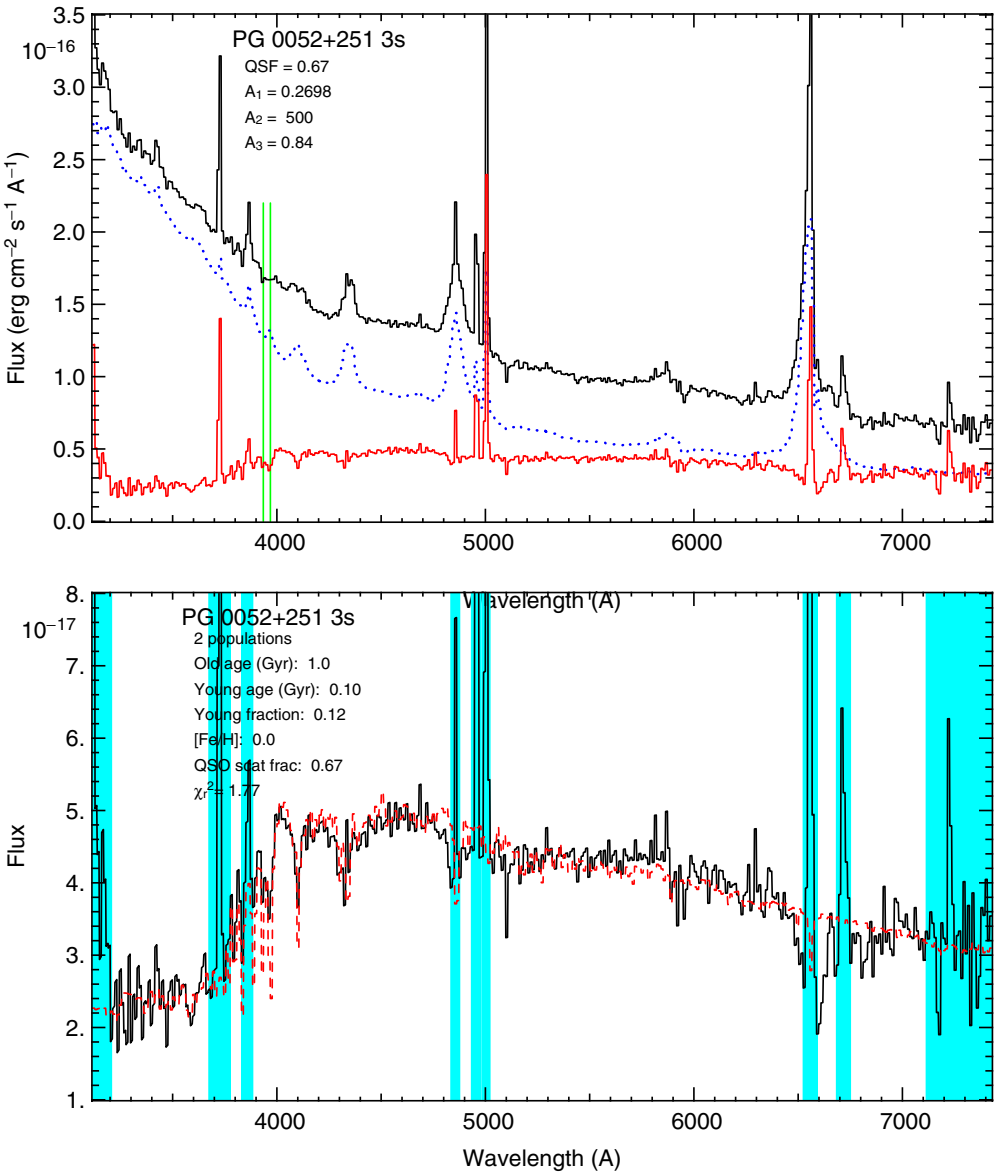

Figure 5. Problematic quasar emission line from Ne III at 3969 Å affecting the Ca H&K region for PG 0052+251. The QSO scattered light subtraction is shown on top (legend is the same as in Figure 3) and the simultaneously best-fitting stellar-population model on the bottom. The Ca H&K lines (marked by green vertical lines in the top plot) appear affected.

(A color version of this figure is available in the online journal.)

section are from Bahcall et al. (1997) except for 4C 31.63, which is from Hamilton et al. (2002), and PKS 0736+017, which is from Dunlop et al. (2003). All quoted velocity dispersions are aperture-corrected values. Stellar populations are qualitatively mentioned, based on the model fitting performed during our scatter subtraction process. More accurate stellar populations will be analyzed in future work. Where relevant, implied star-formation rates from the [O II] line emission in the entire host galaxies are taken from Ho (2005). For reference, mean galaxy parameters for the different types of objects are given in Table 5.

3.3.1. PG 0052+251

PG 0052+251 (labeled 1 in our plots) is an RQ quasar with $M_V = -24.1$ and $L_{5\,\mathrm{GHz}} = 2.4 \times 10^{39}$ erg s^{-1}. The host galaxy, at $M_V = -22.5$, is obviously a spiral in the *HST* images and was classified as such by both Bahcall et al. (1997) and Hamilton et al. (2002) (also studied by Boroson et al. 1982; Boroson et al. 1985; Stockton & MacKenty 1987; Hutchings et al. 1989; Dunlop et al. 1993; McLeod & Rieke 1994; Bahcall et al. 1996). It has a companion at a distance of 14.″1. Bahcall et al. (1997) suggest that this galaxy is an Sb spiral with a fairly large bulge component, best fitted by an exponential disk two-dimensional profile.

This host galaxy is the smallest ($R_e = 4.8$ kpc) and brightest ($\mu_e = 19.35$ mag arcsec^{-1}) of our sample. It lies within the early-type galaxy FP and has properties consistent with the Dasyra et al. (2007) PG QSO hosts. Its velocity dispersion has an upper limit of 279 km s^{-1}. The galaxy spectrum contains many emission lines indicating ongoing star formation and no significant old stellar population. Furthermore, Bahcall et al. (1997) observed 11 bright H II regions in the *HST* image. Ho (2005) estimates a star-formation rate of 3.7 $M_\odot$ yr^{-1} from the [O II] luminosity. We estimate a young effective age for this galaxy.

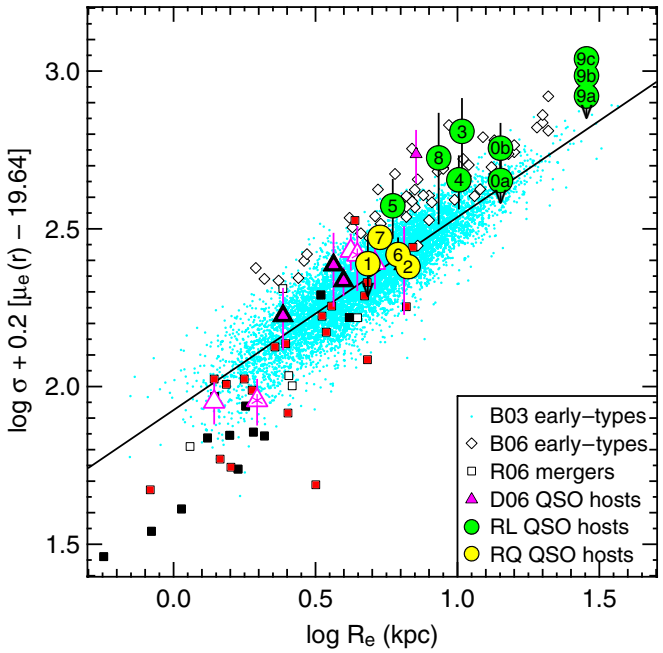

Figure 6. The FP using the projection from Bernardi et al. (2006). QSO host galaxies from this work are shown as large circles (RL are green, RQ are yellow, the numbers correspond to object numbers in the tables, with 10a and 10b marked as 0a and 0b), RQ PG QSO hosts from Dasyra et al. (2007) are triangles coded by morphology (the large filled triangles are ellipticals, the crosses denote ellipticals with signs of interaction (underneath other symbols in this plot; can be seen in Figure 7), the large open triangles are early-types, the large open triangles with asterisks are spirals, and the small filled triangles are unknown), merger remnant galaxies from Rothberg & Joseph (2006) are squares (normal mergers are the filled red squares, LIRG/ULIRGs are the filled black squares, and shell ellipticals are the open squares), early-type galaxies from Bernardi et al. (2003a) are the small dots, and early types with $\sigma_* > 350$ km s^{-1} from Bernardi et al. (2006) are the diamonds.

(A color version of this figure is available in the online journal.)

3.3.2. PHL 909 (0054+144)

PH 909 (labeled 2 in our plots) is an RQ quasar with $M_V = -24.1$ and $L_{5\,\mathrm{GHz}} = 1.1 \times 10^{40}$ erg s^{-1}. Unlike our other RQ hosts, this one is a normal E4 elliptical galaxy with $M_V = -22.2$ and has a companion of ∼12 arcsec to the west. Extended emission toward this companion was noted by Dunlop et al. (1993) and Gehren et al. (1984), but not by Bahcall et al. (1997).

This host galaxy has our smallest measured velocity dispersion (167 km s^{-1}) that is also at the low end of the Dasyra et al. (2007) PG QSO sample. Its effective radius (6.7 kpc) lies in the transition region between our RQ and RL objects. Its surface brightness (20.4 mag arcsec^{-1}) is lower than the rest of our RQ hosts and near the mean of our RL hosts. The stellar mass ($2.2 \times 10^{11}\ M_\odot$) and M/L (3.8) are the lowest of our sample. Its spectrum shows [O II] emission and looks to be of intermediate age.

3.3.3. PKS 0736+017

PKS 0736+017 (labeled 3 in our plots) is an RL, compact, flat-spectrum quasar (Gower & Hutchings 1984; Romnev et al. 1984) with $M_V = -23.2$ and $L_{5\,\mathrm{GHz}} = 9.0 \times 10^{42}$ erg s^{-1}. The host galaxy ($M_V = -22.7$) shows a disturbed morphology with nebulosity extending to nearby companions (Dunlop et al. 1993).

This host galaxy's velocity dispersion (342 km s^{-1}) is above average for the RL hosts. The effective radius (10.4 kpc) and surface brightness (21.0 mag arcsec^{-1}) are slightly below average. It sits high on the FP for its size. The stellar mass ($14.1 \times 10^{11}\ M_\odot$) is near the mean of the RL hosts, while its M/L (17.8) is above average. The spectrum shows no emission lines and can be fitted by an intermediate-aged population.

3.3.4. 3C 273 (PG 1226+023)

3C 273 (labeled 4 in our plots) is the most luminous quasar in our sample, both in the optical ($M_V = -26.7$) and the radio ($L_{5\,\mathrm{GHz}} = 1.3 \times 10^{44}$ erg s^{-1}). It has a large radio jet that is also weakly detected in the optical *HST* images (Bahcall et al. 1997). The host galaxy is classified as an elliptical by Bahcall et al. (1997) and Hamilton et al. (2002) with $M_V = -23.2$. There are no nearby companion galaxies.

This galaxy has a velocity dispersion of 334 km s^{-1}, falling at the low end of the distribution of Bernardi et al. (2006) massive elliptical galaxies, but slightly above average for our RL hosts. Its surface brightness (20.3 mag arcsec^{-1}) is slightly fainter than the mean of the Bernardi et al. (2003a) normal early-type galaxies. Its effective radius is above average (10.1 kpc), but well within the distribution of normal early-type galaxies and near the mean of our six RL objects and of the massive early types. The M/L (9.1) is above the normal and lower than the massive early-type galaxies. Its spectrum shows [O II] emission, but can be fitted by a relatively old single population.

3.3.5. PKS 1302-102

PKS 1302-102 (labeled 5 in our plots) is an RL, flat-spectrum, quasar at $M_V = -25.9$ and $L_{5\,\mathrm{GHz}} = 9.5 \times 10^{42}$ erg s^{-1}. The host galaxy, at $M_V = -22.9$, is classified as an elliptical that may be slightly disturbed by two companions within 2.″3 (Hutchings & Neff 1992; Bahcall et al. 1997; Hamilton et al. 2002; Guyon et al. 2006). Bahcall et al. (1997) visually classify this galaxy as an E4; however, they find that an exponential disk profile best fits the PSF-subtracted image. Guyon et al. (2006) comment on the difficulty of decoupling the host and its closer companion, but find that their two-dimensional fit favors an $r^{1/4}$ model.

On the FP, this host occupies a transition region between our RL and RQ objects. Its velocity dispersion (388 km s^{-1}) is on the high end of our RL hosts; however, the surface brightness (19.56 mag arcsec^{-1}) is higher than all other RL hosts, and near that of our RQ QSO hosts. Its size ($R_e = 5.9$ kpc) is comparable to the RQ hosts as well. The M/L (10.3) and stellar mass ($10.3 \times 10^{11}\ M_\odot$) are on the low end of the RL objects, but larger than the RQ objects. This stellar mass is similar to the massive early-type galaxies, however, the M/L is slightly lower. The spectrum shows [O II] in emission, but the 4000 Å break region suggests a fairly old stellar population. Current data quality does not allow a secure fit over the rest of the spectrum.

3.3.6. PG 1309+355

PG 1309+355 (labeled 6 in our plots) could be called a radio-intermediate quasar. It falls into the category of RQ using the Kellermann et al. (1994) cut at $L_{5\,\mathrm{GHz}} \sim 10^{26}$ W Hz^{-1}, but is classified as RL using the criterion of radio-to-optical flux density ratio greater than 10 (Brinkmann et al. 1997; Yuan et al. 1998; Hamilton et al. 2002). The absolute magnitude of the quasar is $M_V = -24.4$ and the radio luminosity is $L_{5\mathrm{GHz}} = 1.8 \times 10^{41}$ erg s^{-1}. The host galaxy, at $M_V = -22.8$, is classified

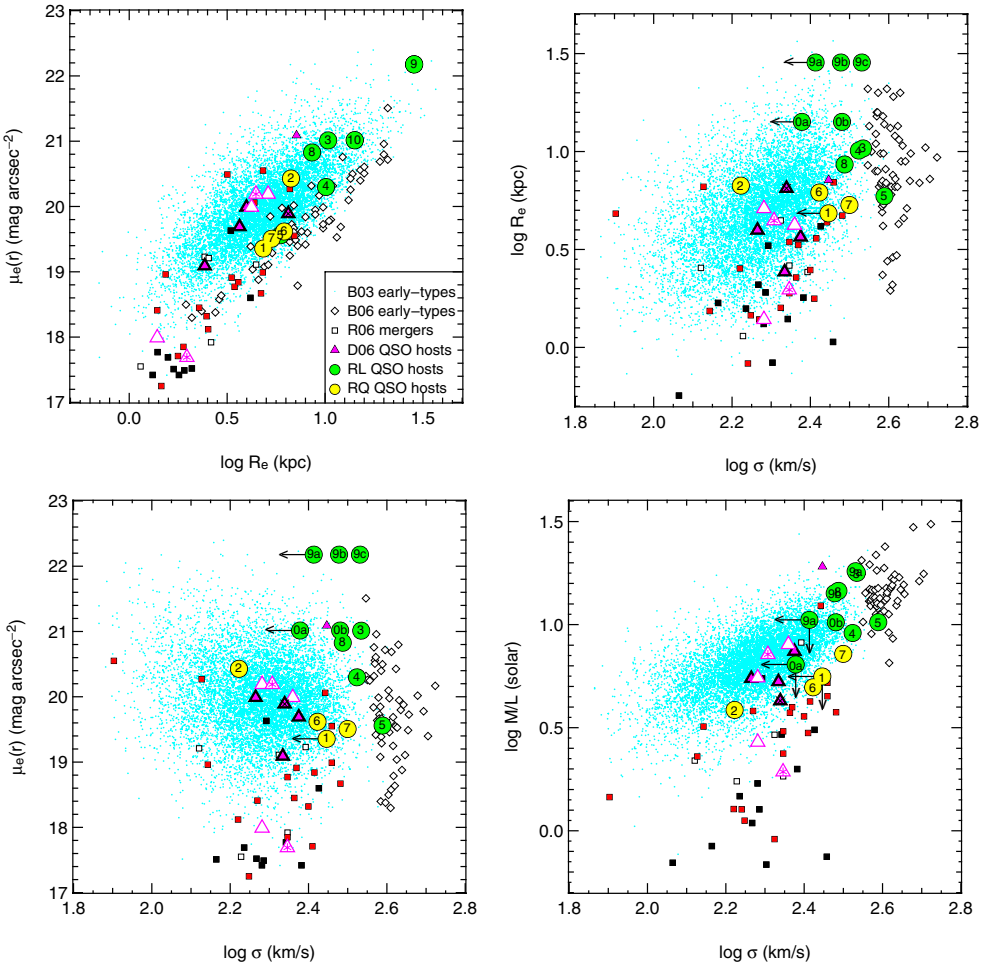

Figure 7. Fundamental galaxy parameters. The symbols are the same as in Figure 6. Note that (1) is upper limits on σ_* and M. (A color version of this figure is available in the online journal.)

Table 5
Mean Galaxy Parameters

Group	R_e (kpc)	σ_* [a] (km s^{-1})	$\mu_e(r)$ (mag arcsec^{-1})	M/L ($M_\odot/L_\odot$)	M_* ($10^{11}\,M_\odot$)	References
(1)	(2)	(3)	(4)	(5)	(6)	(7)
Our QSO hosts	9.2	291.6[b]	20.5	10.0[b]	11.3[b]	This work
RL hosts	11.4	320.9	20.8	12.4	14.8	This work
RQ hosts	6.0	240.8[b]	19.8	5.3[b]	4.4[b]	This work
PG QSO hosts	3.6	183	19.6	4.8	1.7	Dasyra et al. (2007)
Early-type galaxies	4.9	190	20.0	7.0	2.1	Bernardi et al. (2003a)
High σ early-type galaxies	8.0	403	19.8	14.7	12.2	Bernardi et al. (2006)
Merger remnants	2.2	190	18.2	2.8	1.5	Rothberg & Joseph (2006)

Notes.
[a] Aperture-corrected values.
[b] Excluding PG 0052+251, for which we only have upper limits.

as an early-type spiral by Bahcall et al. (1997) and Hamilton et al. (2002) and as a moderately elongated elliptical by Guyon et al. (2006). The *HST* images show tightly-wrapped spiral arms. There are no nearby companions.

This galaxy has a high effective radius (6.2 kpc) for our RQ hosts, which is equal to the highest of the Dasyra et al. (2007) PG QSO hosts, lies well below the average of our RL hosts, and is between the means of the normal and massive quiescent early-type galaxies. The velocity dispersion (265 km s^{-1}) falls at the high end of the distribution of Dasyra et al. (2007) PG QSO hosts and above the mean of the normal early-type galaxies. The surface brightness (19.62 mag arcsec^{-2}) is near the mean of our RQ hosts and of the Dasyra et al. (2007) PG QSO hosts. The M/L (5.0) and stellar mass ($5.0 \times 10^{11}\,M_\odot$) are the lowest of our host galaxy sample. Its M/L is very close to the Dasyra et al. (2007) PG QSO hosts, while its stellar mass is higher than the means of the PG QSO hosts, the merger remnants, and the normal early-type galaxies. The host galaxy spectrum shows the [O II] emission, but is fitted well by an old population.

3.3.7. PG 1444+407

PG 1444+407 (labeled 7 in our plots) is an RQ quasar with $M_V = -25.3$ and $L_{5\,\mathrm{GHz}} = 1.8 \times 10^{39}$ erg s^{-1}. The QSO spectrum is similar to that of 4C 31.63, showing a strong Fe II emission, broad Balmer lines and no detectable forbidden emission lines. The host galaxy, at $M_V = -22.7$, appears smooth and elongated in the north–south direction in the *HST* images of Bahcall. They suggest that the host galaxy has the appearance of an E1, although the light profile is better fitted by an exponential disk. It is classified as a spiral galaxy by Hamilton et al. (2002) and a bar may be present (Hutchings & Neff 1992; Bahcall et al. 1997).

The size ($R_e = 5.3$ kpc) of this host galaxy is near the average of the normal early-type galaxies and slightly higher than the Dasyra et al. (2007) PG QSO hosts. Its velocity dispersion (316 km s^{-1}) is the highest of our RQ hosts and near the mean of our RL hosts, though its stellar mass ($6.4 \times 10^{11}\ M_\odot$) is much lower than the RL hosts. Its surface brightness (19.51 mag arcsec^{-1}) is near that of our other RQ QSO hosts, brighter than our RL hosts, and about average compared to the Dasyra et al. (2007) PG QSO hosts. The spectrum can be fitted with about 3/4 of the light from a moderately young population and the rest old. [O II] is in emission and Ho (2005) estimates a star-formation rate of 19.4 $M_\odot$ yr^{-1} from the [O II] luminosity.

3.3.8. PKS 2135-147

PKS 2135-147 (labeled 8 in our plots) is an RL quasar with $M_V = -24.7$ and $L_{5\,\mathrm{GHz}} = 7.7 \times 10^{42}$ erg s^{-1}. The host galaxy ($M_V = -22.4$) is classified as an elliptical with two companions within 5.″5 (Bahcall et al. 1997; Hamilton et al. 2002).

The size of this host ($R_e = 8.6$ kpc) is average for our sample, but slightly above the average of the high-mass early-type galaxies. Its surface brightness (20.83 mag arcsec^{-1}) is average for our RL hosts, but lower than all other groups of objects. The velocity dispersion (307 km s^{-1}) is slightly below average for the RL hosts. The M/L (14.6) is average for our RL sample and the stellar mass ($9.4 \times 10^{11}\ M_\odot$) is on the low end of the RL hosts. The spectrum shows many emission lines, suggesting the ongoing star formation; however, we are not able to make an estimate of this galaxy's stellar populations with our current data quality.

3.3.9. 4C 31.63 (2201+315)

4C 31.63 (labeled 9 in our plots) is an RL quasar at $M_V = -25.1$ and $L_{5\,\mathrm{GHz}} = 1.9 \times 10^{43}$ erg s^{-1}. It has the spectrum of a typical strong Fe II object. The host galaxy is one of the few objects in our larger sample, and the only object in this subsample, that is clearly a first-rank elliptical at $M_V = -23.8$. This galaxy is classified as a smooth elongated elliptical from both optical *HST* images (Bahcall et al. 1997; Hamilton et al. 2002) and ground-based near-infrared AO images (Guyon et al. 2006) with three apparent companions within 5″ of the QSO.

This is our most extreme host galaxy on the FP, lying in the upper-right corner. It has the largest effective radius of our objects (28.8 kpc) and, correspondingly, the lowest surface brightness (22.18 mag arcsec^{-1}). Its velocity dispersion measured in three locations ranges from 259 to 339 km s^{-1}, but is consistent within the error bars. The average measured σ_* gives a mass of $30.1 \times 10^{12}\ M_\odot$, the highest of our sample. The M/L (14.3) is typical of the massive early-type galaxies. The host galaxy spectrum clearly reveals an old galaxy with no emission lines. We estimate an old population with no apparent signs of a younger one. This is the only host galaxy in our sample with the purely old spectrum typical of a giant elliptical.

3.3.10. PKS 2349-014

PKS 2349-014 (labeled 10 in our plots) is an RL quasar at $M_V = -24.5$ and $L_{5\,\mathrm{GHz}} = 2.9 \times 10^{42}$ erg s^{-1}. The QSO has a typical spectrum with strong broad permitted lines and much narrower forbidden lines with a modest amount of Fe II emission. The host galaxy ($M_V = -23.2$) appears very disturbed, although the radial profile is well described by an $r^{1/4}$ model (Bahcall et al. 1997; Hamilton et al. 2002). This galaxy shows obvious morphological signs of gravitational interaction, such as large tidal arms and extensive diffuse, off-center nebulosity. Bahcall et al. (1995) identify several distinct regions for which we have obtained spectra: the diffuse nebulosity 3″ south of the nucleus and the "wisps" (possible tidal feature) 4″ north of the nucleus.

The velocity dispersions of these two components are the same within error bars, at <250 and 302 km s^{-1}, respectively, and are near the average of our QSO host galaxy sample. The host galaxy surface brightness (21.02 mag arcsec^{-1}) is below the average of our RL objects and of the massive early-type galaxies. Its effective radius (14.1 kpc) is the second highest in our sample and is larger than the average massive early-type galaxy. The M/L (8.3) and stellar mass ($12.2 \times 10^{11}\ M_\odot$) are slightly below the averages of the RL hosts. The spectra of the two regions show a number of emission lines. They can be fitted by an underlying old population with 20–50% moderately young. Ho (2005) estimates a star-formation rate for this host galaxy of 8.3 $M_\odot$ yr^{-1} from the [O II] luminosity.

4. DISCUSSION

4.1. The Exponential Disk Galaxies

Although we have thus far utilized the parameters of our QSO host galaxies that were derived from two-dimensional $r^{1/4}$ profile fits, Bahcall et al. (1997) actually found that four galaxies were better fitted by an exponential disk model: PG 0052+251, PG 1444+407, PG 1309+355, and PKS 1302-102. The first three of these show obvious spiral structure and the fourth one is described as a disturbed elliptical. We now analyze the properties derived from exponential disk fits to these four galaxies. Placement of disk galaxies on the FP is not technically correct since this relation holds only for early-type galaxies and bulges. Nonetheless, we do it here to investigate the range in which these galaxies should fall, given that they are likely to have a bulge component and that our velocity dispersion measurements may have contained light from both the disk and the bulge. Therefore, these galaxies should exist somewhere between the positions of pure bulge and pure disk.

Table 6 gives the exponential disk parameters derived by Bahcall et al. (1997) and our galaxy properties calculated from them. We convert Bahcall's disk scale lengths, R_s, to effective radii, R_e, using $R_e = 1.6785\ R_s$ (de Vaucouleurs & Pence 1978). The new galaxy positions (for objects 1, 5, 6, and 7) are shown on the FP in Figure 8 and on galaxy parameter plots in Figure 9. The lines connected to the new points illustrate the range between the new exponential disk model locations and the previous $r^{1/4}$ model locations for these galaxies. It can be seen in Figure 8 that all four host galaxies move up on the FP. Interestingly, PKS 1302-102, the RL QSO, now resides among the loci of the RL objects, rather than appearing to

Table 6
Host Galaxy Properties from Exponential Disk Fits

Object # (1)	Object Name (2)	M_V(host) (mag) (3)	R_e (arcsec) (4)	R_e (kpc) (5)	$\mu_e(r)$ (mag arcsec^{-1}) (6)	M/L ($M_\odot/L_\odot$) (7)	M_* ($10^{11}\,M_\odot$) (8)
1	PG 0052+251	17.51	2.2	5.9	20.27	<10.8	<5.3
5	PKS 1302 − 102	18.70	1.8	7.8	20.66	21.5	13.6
6	PG 1309+355	17.65	2.0	6.2	20.13	7.9	5.1
7	PG 1444+407	18.87	1.7	6.9	20.66	16.2	8.0

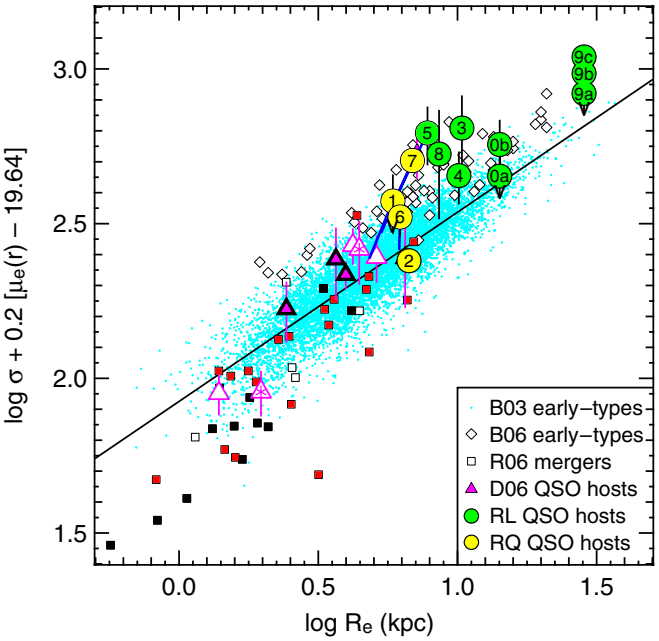

Figure 8. The FP using galaxy parameters derived from exponential disk profile fits for PG 0052+251 (1), PKS 1302-102 (5), PG 1309+355 (6), and PG 1444+407 (7). The lines connected to these points show the spread between the exponential disk positions and the $r^{1/4}$ positions. Otherwise, the symbols are the same as in Figure 6.

(A color version of this figure is available in the online journal.)

exist in a transition region between the RL and RQ groups. The RQ QSOs have also moved up into the region occupied by massive early-type galaxies. Their masses derived from the new radii, also given in Table 6, are indeed all well above $10^{11}\,M_\odot$. Regardless of assumed morphology, these are massive galaxies. It can be seen in Figure 9 that these four RQ galaxies now lie among the largest, lowest surface brightness, and highest M/L QSO hosts from Dasyra et al. (2007). However, it is expected that disk galaxies in that sample would move similarly if exponential disk models were used to derive their parameters.

4.2. Is Location on the Fundamental Plane Related to Host Galaxy Morphology?

Of the six RL objects in our sample, all are morphologically classified (Table 1) as elliptical galaxies except for PKS 2349-014 and PKS 0736+017, which are complex and interacting with clear tidal tails, nevertheless well fit by a $r^{1/4}$ light distribution. Bahcall et al. (1997) and Schweizer (1996) suggest that PKS 2349-014 may be a proto-elliptical galaxy resulting from a merger of two spirals. PKS 1302-102, PKS 2135-147, PKS 2349-014, and 4C 31.63 all have companions within 5″ of the QSO. Of the four RQ objects, PG 0052+251 is classified as an Sb galaxy and shows HII regions; PG 1444+407 is classified as an E1 by Bahcall et al. (1997), as a spiral by Hamilton et al. (2002), and may contain a bar (Hutchings & Neff 1992; Bahcall et al. 1997); PG 1309+355 is an Sab with tightly wound spiral arms; and PHL 909 is clearly an elliptical galaxy. PHL 909 is our only RQ host with a nearby companion.

Our QSO hosts at the upper envelope of the FP are either elliptical or interacting galaxies. Three RQ spiral galaxies and one elliptical lie on the FP. If we also consider the Dasyra et al. (2007) QSO hosts, ellipticals, interacting ellipticals, early-types, and spirals all lie on the FP close to our four RQ hosts. An early-type and spiral also lie well below the FP among the merger remnants. This lack of morphological consistency suggests that host galaxy morphology alone is not the driver of the position on the FP or in the galaxy property plots of Figure 7 for this small sample.

4.3. Evolution or Different Populations?

If we look at the different groups of objects in the plots of Figures 6 and 7, we see trends suggesting different classes of galaxies. First we address the general trends. All objects—quiescent early-type galaxies, massive early-type galaxies, quasar host galaxies, and galaxy merger remnants—lie nearly on the FP (or are expected to lie there once faded, in the case of the merger remnants). Of course, we expect the early-type galaxies, including QSO hosts of that morphology, to be there. The RL hosts lie among the massive early-type galaxies at the upper edge of the plane. The merger remnants were morphologically chosen to be near the end of the merger sequence with the stipulation that the cores have already coalesced into a single nucleus. Since we believe that early-type galaxies form from mergers, it is not surprising that these also occupy the FP. The LIRG/ULIRGs have a slight offset below the plane due to their currently high luminosity, but are expected to fade up to the FP after the starbursts end. The RL quasar hosts are morphologically either early-type or interacting and on their way to forming early types, and, therefore, they would be expected on the FP. Perhaps the hardest to explain are the RQ QSO hosts that show definite signs of spiral structure (three of our RQ objects and two of the Dasyra et al. 2007 sample).

The upper-left plot of Figure 7 shows surface brightness and effective radius. The merger remnants tend to be small and bright, suggesting that nuclear starbursts are in progress. The massive early-type galaxies from SDSS are bright and mostly large, though a few stretch down to small radii. The Dasyra et al. (2007) QSO hosts tend to have lower surface brightness for a given radius than either the massive galaxies or the merger remnants, residing near the center of the distribution of normal early-type galaxies from SDSS. Our three RQ hosts that are

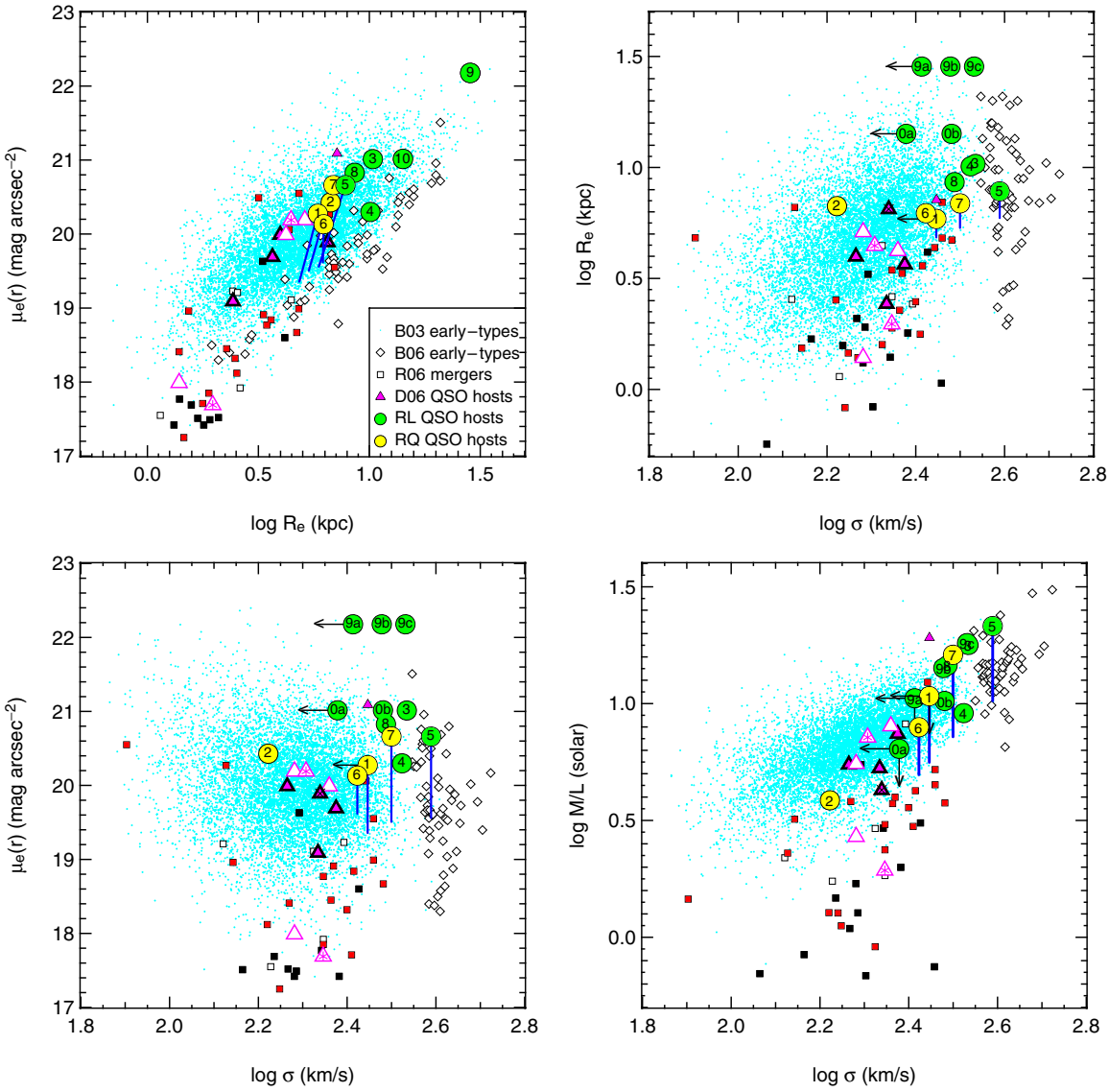

Figure 9. Fundamental galaxy parameters derived from exponential disk profile fits for PG 0052+251 (1), PKS 1302-102 (5), PG 1309+355 (6), and PG 1444+407 (7). The symbols are the same as in Figures 6 and 8.

(A color version of this figure is available in the online journal.)

spirals lie in the transition region between normal and massive early-type quiescent galaxies, while the elliptical host resides up among the normal quiescent early types.

In the upper-right plot of Figure 7, the stellar velocity dispersions of the merger remnants and the lower-luminosity RQ QSO hosts overlap and fall well within the distribution of normal early-type galaxies, as concluded by Dasyra et al. (2007). It has been suggested that LIRG/ULIRGs form intermediate-sized elliptical galaxies from the merger of two gas-rich spiral galaxies and will not evolve into the brightest QSOs (Genzel et al. 2001; Tacconi et al. 2002; Rothberg & Joseph 2006; Dasyra et al. 2006). This idea is supported by the similar velocity dispersions of these two classes of objects, and by their mass-to-light ratios (the lower-right plot of Figure 7; note that most of our RQ QSO hosts are on the high end of the other PG QSO hosts in σ_* and M_*). The merger remnants have a lower M/L due to their currently high luminosities, but after fading should reside among the lower-luminosity RQ QSO hosts in Figures 6 and 7. There is a clear distinction between these objects and our massive RL QSO hosts in σ_* and R_e (and thus stellar mass). The separation occurs at $\sigma_* \sim 300$ km s^{-1}, $R_e \sim 6$ kpc, and corresponding $M_* \sim 7 \times 10^{11}\, M_\odot$. Such a distinction between RL and RQ QSOs has been observed as a function of estimated black hole mass (Dunlop et al. 2003), however, here we have deduced it using directly measured host galaxy stellar velocity dispersions.

Because our method of calculating galaxy mass assumes that the velocity anisotropies are small and that the system is dynamically hot (Bender et al. 1992), the masses calculated in this way for spiral galaxies or those with strong interactions will be systematically incorrect. We now consider only the galaxies that are known to have elliptical morphologies. The RQ elliptical QSO host sample consists of PHL 909, PG 0007+106, PG 1617+175, and PG 2214+139 (the last three are from Dasyra et al. 2007), while the RL sample includes 3C 273, PKS 2135-147, and 4C 31.63. Our calculated masses for the RQ group of ellipticals are 1.3–2.4 $\times$ $10^{11}\, M_\odot$ with an average of 1.9 $\times$ $10^{11}\, M_\odot$. The RL group has calculated masses of 9.4–29.8 $\times$ $10^{11}\, M_\odot$ with an average of 17.4 $\times$ $10^{11}\, M_\odot$. This gives an RL/RQ division somewhere between 2.4–9.4 $\times$

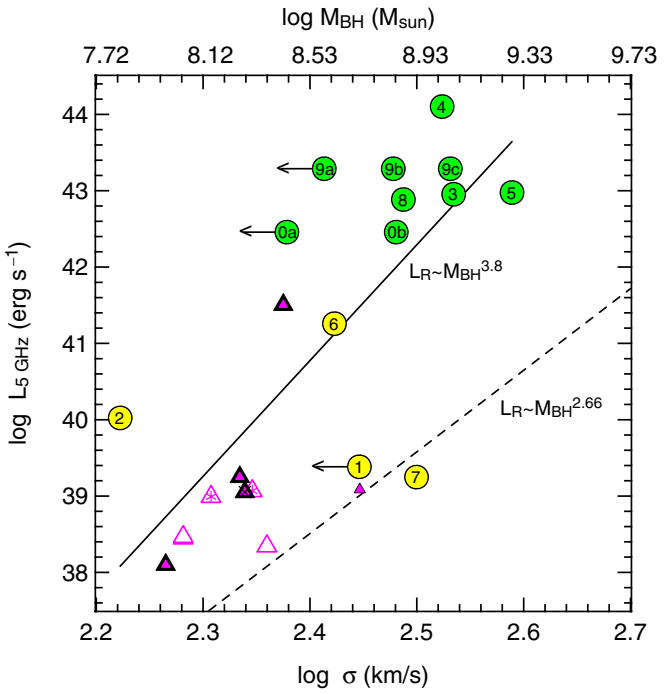

Figure 10. Radio luminosity as a function of stellar velocity dispersion and black hole mass. The symbols are the same as in Figure 6. $M_{\rm BH}$ was calculated from the Tremaine et al. (2002) $M_{\rm BH}$–σ relation using our measured σ_*. The solid line is the best linear regression fit to our objects and the lower luminosity Dasyra et al. (2007) QSOs (excluding PG 0052+251, #1). The dashed line is the Franceschini et al. (1998) $L_{5\ \rm GHz} \propto M_{\rm BH}^{2.66}$ linear regression, derived for nonactive galaxies over log $M_{\rm BH} \sim$ 6.2-9.5 $M_\odot$.

(A color version of this figure is available in the online journal.)

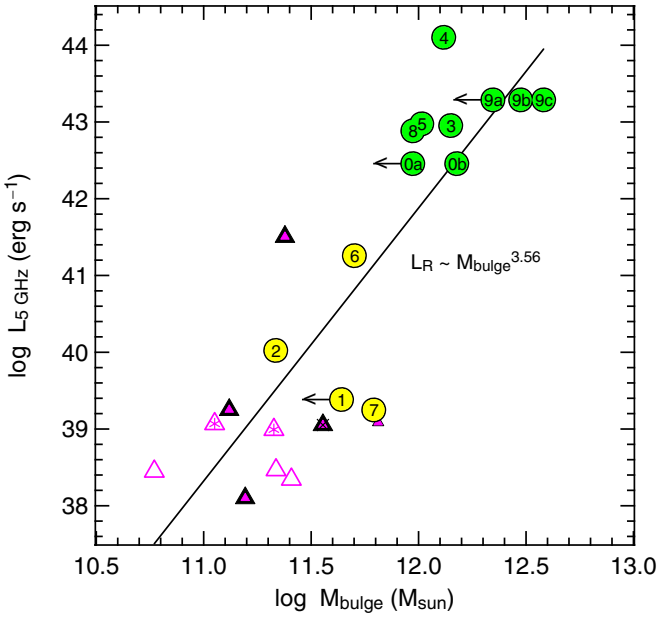

Figure 11. Radio luminosity as a function of galaxy bulge mass (calculated from directly measured host galaxy σ_* and $R_{\rm eff}$). The solid line is a fit to the data, excluding PG 0052+251, #1.

(A color version of this figure is available in the online journal.)

$10^{11}\ M_\odot$, or $M_* \sim 5.9 \pm 3.5 \times 10^{11}\ M_\odot$, for the elliptical QSO host galaxies.

Mean galaxy parameters are given in Table 5 for the different groups of galaxies. Overall, our RQ hosts show properties similar to normal early-type galaxies, though slightly larger and more massive. A comparison of properties of our RQ hosts and normal early-type galaxies show R_e = 5.7, 4.9 kpc, respectively, M/L = 5.3, 7.0, σ_* = 241, 190 km s^{-1}, and M_* = 4.4, 2.1 $\times$ $10^{11}\ M_\odot$. However, our RL hosts are more analogous to the massive early-type galaxies. They are larger (11.4, 8.0 kpc, respectively) with lower surface brightness (20.8, 19.8 mag arcsec^{-1}), lower σ_* (321, 403 km s^{-1}) and M/L (12.4, 14.7), but higher M_* (14.8, 12.2 $\times$ $10^{11}\ M_\odot$). It appears that we have two classes of objects, regardless of the surface brightness model used for the disk galaxies (refer also to Figures 8 and 9): very massive galaxies with RL quasars and intermediate-mass galaxies with RQ quasars. This supports the conclusions of Malkan (1984) who found in an imaging study that RQ quasars have the color, size, surface brightness, and scale length of normal early-to-intermediate-type spiral galaxies, while RL quasars appear to reside in moderate to bright ellipticals.

4.4. Radio Properties

We see in Figures 6 and 7 that all RL QSO hosts reside among the massive early-type galaxies. A more detailed look at the radio properties of these objects reveals a correlation between radio luminosity and σ_*, shown in Figure 10 with 5 GHz radio fluxes taken from Kellermann et al. (1994) and the NASA/IPAC Extragalactic Database (modified to our adopted cosmology of $\Omega_M = 0.3$, $\Omega_\Lambda = 0.7$, $H_0 = 70$ km s^{-1} Mpc^{-1}).

A similar correlation was found by Nelson & Whittle (1996) for RQ Seyfert galaxies, which extended to higher luminosity radio galaxies when considering the core radio emission. They interpreted this correlation as a dependence of radio emission on galaxy bulge mass.

Subsequent studies (Franceschini et al. 1998; McLure et al. 1999; Nelson 2000; Laor 2000; Lacy et al. 2001; Ho 2002; Dunlop et al. 2003; Snellen et al. 2003; McLure & Jarvis 2004; Woo et al. 2005) have looked at the dependence of radio luminosity on black hole mass ($M_{\rm BH}$), which we now know is related to σ_* and galaxy bulge mass (Gebhardt et al. 2000a; Ferrarese & Merritt 2000). Franceschini et al. (1998) found a tight dependence of $L_{5\ \rm GHz} \propto M_{\rm BH}^{2.66}$ for a sample of 13 nearby early-type galaxies with $M_{\rm BH}$ estimated from stellar or gas kinematics. There has been some disagreement on this correlation as different types of objects were analyzed (McLure et al. 1999; Lacy et al. 2001; Ho 2002; Snellen et al. 2003; Woo et al. 2005; McLure & Jarvis 2004) and scatter about the relation grew to several orders of magnitude when AGNs of different activity levels were added. For these larger samples, a wide range of radio luminosity is possible for a given $M_{\rm BH}$ and it is likely more dependent on BH accretion rate than on the mass (Ho 2002). Ho (2002) suggested that the $L_{\rm radio}$–$M_{\rm BH}$ relation arises indirectly through more fundamental correlations between radio luminosity and bulge mass and between bulge mass and black hole mass, similar to the original interpretation of Nelson & Whittle (1996). For strongly active quasars, we find a tighter correlation of radio luminosity with host galaxy bulge mass (calculated from directly measured host galaxy parameters) than with black hole mass (inferred from the Tremaine et al. 2002 $M_{\rm BH}$–σ relation). This relationship is shown in Figure 11. Our best linear regression fit to the data gives the relation $L_{\rm radio} \sim M_{\rm bulge}^{3.56}$ with an rms scatter of 1.09 dex.

One consensus that has arisen from all of these studies is that RL AGNs almost exclusively have $M_{\rm BH} \geqslant 10^8\ M_\odot$. Indeed all of our RL quasars in Figure 10 have $M_{\rm BH} > 10^8\ M_\odot$. The best-fit line to the QSO hosts of this work and of Dasyra

et al. (2007) suggests a steeper slope of $L_{5\,\mathrm{GHz}} \propto M_{\mathrm{BH}}^{3.8}$ with an rms scatter of 1.36 dex; however, given our limited sample size, the small M_{BH} range covered by the data, the large scatter associated with this relation, and possible differences in black hole mass estimation techniques (the black hole masses of the QSOs in this study and their place on M_{BH}–σ relation will be discussed in future work), the QSOs in this study are consistent with the previously determined $L_{5\,\mathrm{GHz}}$–M_{BH} correlation. Like the host galaxy parameters in Section 4.3, radio emission has a dependence on the mass of either the host galaxy and/or the central black hole. Our data on active quasars show a stronger dependence on the host galaxy mass.

5. SUMMARY AND CONCLUSIONS

We have for the first time directly measured host galaxy stellar velocity dispersions for very luminous ($M_V < -23$) quasars, including both RL and RQ objects, and analyzed their structural properties. We compare the properties of these host galaxies to those of normal early-type galaxies (Bernardi et al. 2003a), giant early-type galaxies (Bernardi et al. 2006), a sample of RQ PG QSO hosts (Dasyra et al. 2007), and galaxy merger remnants (Rothberg & Joseph 2006). The following summarizes our main conclusions.

1. The six RL QSO host galaxies lie at the upper extreme FP of early-type galaxies. They occupy this location due to their large velocity dispersions (with an average of 321 km s^{-1}), large effective radii (average of 11.4 kpc), low surface brightness (average of 20.8 mag arcsec^{-2}), and high M/L (average of 12.4). The properties of these RL host galaxies are similar to those of giant early-type galaxies in the SDSS, although only one has the spectrum of a purely old giant elliptical galaxy.
2. The four RQ QSO host galaxies reside on the FP among normal early-type galaxies and at the high end of other PG QSO hosts, with a mean velocity dispersion of 241 km s^{-1}. Their surface brightness and effective radii are slightly higher than those of normal early-type galaxies. The M/Ls are slightly below those of normal early-type galaxies.
3. The RL hosts in our study are either elliptical galaxies or interacting, while the RQ hosts show a mixture of spiral and elliptical structures. The distinction between the two groups is due to the galaxy mass, inferred from the measured structural parameters, rather than the morphological galaxy type. The separation occurs at galaxy velocity dispersions of $\sigma_* \sim 300$ km s^{-1}, effective radii of $R_e \sim 6$ kpc, and the corresponding stellar masses of $M_* \sim 5.9 \pm 3.5 \times 10^{11}\ M_\odot$.
4. We confirm a correlation between radio luminosity and stellar velocity dispersion, and thus the implied black hole mass, of the host galaxies that suggests a higher slope ($L_{5\,\mathrm{GHz}} \propto M_{\mathrm{BH}}^{3.8}$ with an rms scatter of 1.36 dex) than that found by Franceschini et al. 1998; ($L_{5\,\mathrm{GHz}} \propto M_{\mathrm{BH}}^{2.66}$), though it could be consistent with previous work given the large scatter in this relation (McLure & Jarvis 2004), our small sample size, the limited M_{BH} range of our data, and differences in M_{BH} estimated from different techniques. We find a tighter correlation between radio luminosity and host galaxy bulge mass, $L_{\mathrm{radio}} \sim M_{\mathrm{bulge}}^{3.56}$ with an rms scatter of 1.09 dex.

M.J.W. was supported by the McKinney Postdoctoral Fellowship at the University of Wisconsin. The authors thank Luis Ho for reading an early draft of this paper and providing very helpful comments, Karl Gebhardt for the use of his velocity dispersion code, and the following people for insightful conversations on various aspects of this work: Eric Hooper, Joseph Miller, and Greg Shields. We would also like to thank the referee, Matt Malkin, for very constructive comments and suggestions that substantially improved the paper.

Facilities: Keck, WIYN, *HST*.

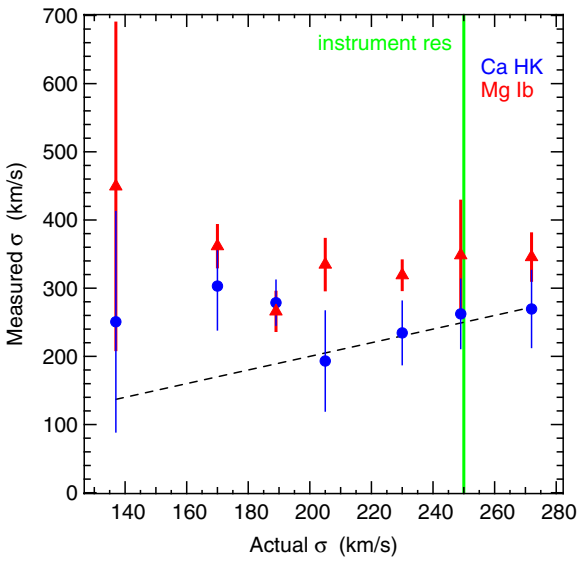

Figure 12. Tests of velocity dispersion measurement limits. Actual σs are from McElroy (1995) and measured σs are our results using the Gebhardt code. The dashed line marks a 1:1 correlation between the two. Circles are measurements on Ca H&K and triangles are on Mg I*b*. Error bars were generated from Monte Carlo simulations. The instrument resolution of the data was 250 km s^{-1}. It is clear that σ measured from the Ca H&K lines is reliable down to 200 km s^{-1}, 20% below the instrument resolution. These tests also show that the Mg I*b* triplet should not be used to measure σ on these data.

(A color version of this figure is available in the online journal.)

Table 7
Measurements on Sigma Standard Galaxies

Galaxy	Actual σ (km s^{-1})	Measured σ (km s^{-1})	Error (km s^{-1})	S/N Å^{-1} (3850–4200 Å)	Galaxy Type
(1)	(2)	(3)	(4)	(4)	(5)
NGC 1407	272	269.5	56.4	2.9	E0
NGC 4594	249	262.3	50.8	6.9	Sa
NGC 584	230	234.4	46.5	4.2	E4
NGC 2768	205	193.2	73.3	4.0	E6
NGC 4579	189	278.7	32.9	5.4	Sb
NGC 3031	170	303.1	64.2	3.5	Sab
NGC 6340	137	250.7	161.5	2.0	S0/a

APPENDIX

MEASUREMENT LIMITS AND SIGMA BIAS

To test our velocity dispersion measurement limitations we used seven standard galaxies from McElroy (1995), a catalog of 86 galaxies with at least three reliable central velocity dispersion measurements in the literature. We used spectra of these galaxies from the STScI database of UV-optical spectra of nearby galaxies (McQuade et al. 1995; Storchi-Bergmann et al. 1995) with instrumental resolution of approximately 250 km s^{-1} and S/N ~ 4 Å^{-1}. The galaxies we used are listed in Table 7 and the fitting results are shown in Figure 12. In this plot, the "actual σs" are from McElroy and "measured σs" are our results from the

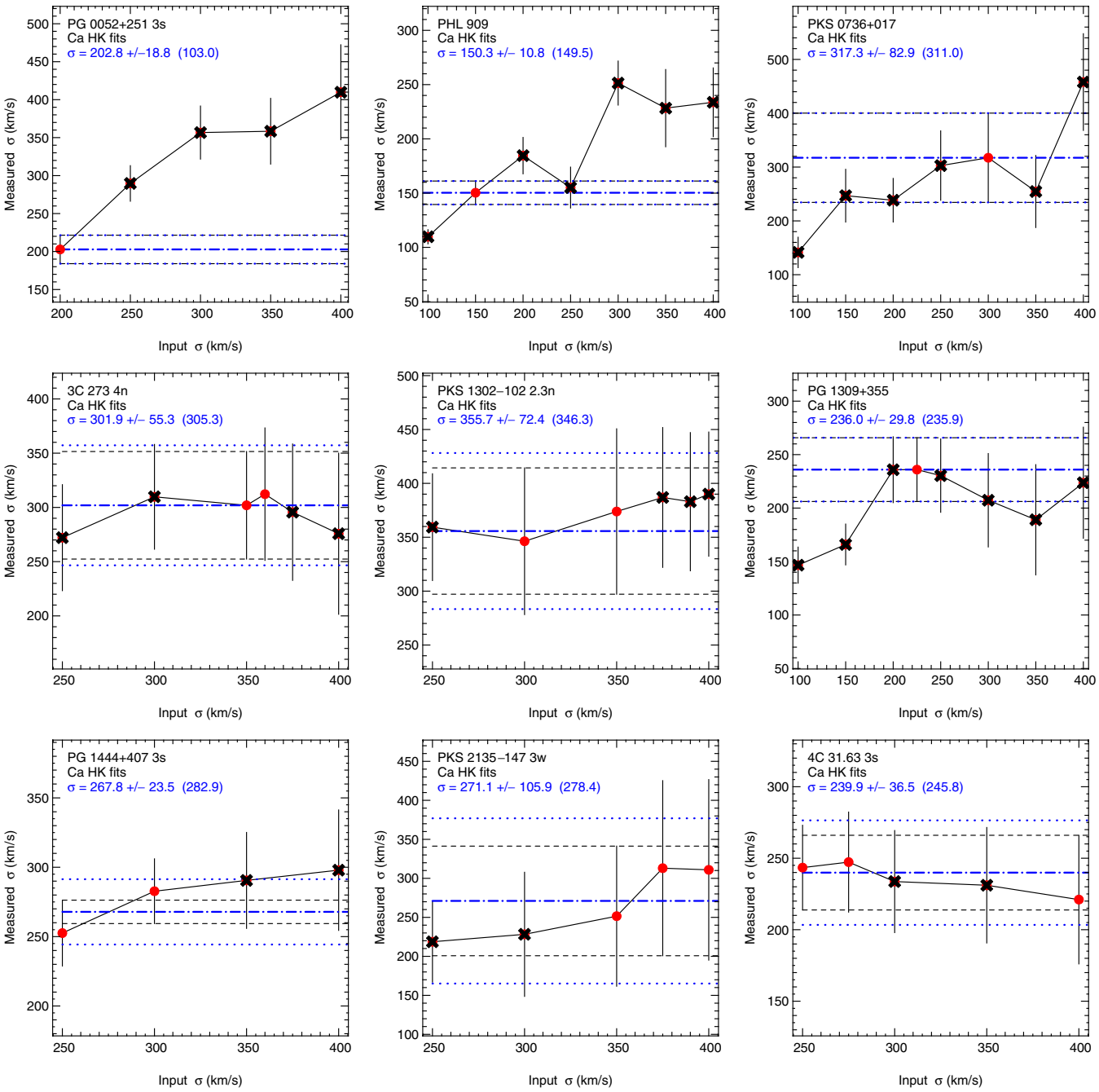

Figure 13. Velocity dispersion measurement tests using a range of input initial σs. Each circle and its error bar is from 100 Monte Carlo simulations at the given input σ. Black crosses mark points for which the sigma bias was >20–40% of the uncertainty. The numbers in parentheses are the interpolated values for zero sigma bias, as demonstrated in Figure 14, and represent our adopted velocity dispersions, except for PG 0052+251 (see text).

(A color version of this figure is available in the online journal.)

Gebhardt code. The dashed line represents a 1:1 correlation between the two. The circles are measurements using the Ca H&K lines and the triangles are measurements using the Mg I*b* triplet. It is clear that results using Ca H&K are good down to 200 km s^{-1}, or 20% below the instrument resolution. These tests also show that the Mg I*b* triplet cannot be used to measure σ_* on these data. For this reason, we used the Ca H&K lines in this work.

Ideally, we should measure the same velocity dispersion of a galaxy regardless of the input initial estimate. However, in the presence of noise, the measurement can be biased. The Gebhardt code evaluates this bias by examining the distribution of measured σ_* values output by the Monte Carlo simulations. If the bias in the distribution is much smaller than the uncertainty, then the measured σ_* is valid.

To investigate the problem of sigma bias, we made measurements on each galaxy using a range of initial input σs. Plots in Figure 13 show the results of these measurements for each of our host galaxies. Each point and error bar represent 100 Monte Carlo simulations of the measurement beginning with that input σ value. Any values where the sigma bias was greater than 20–40% of the uncertainty are marked with crosses and not used.

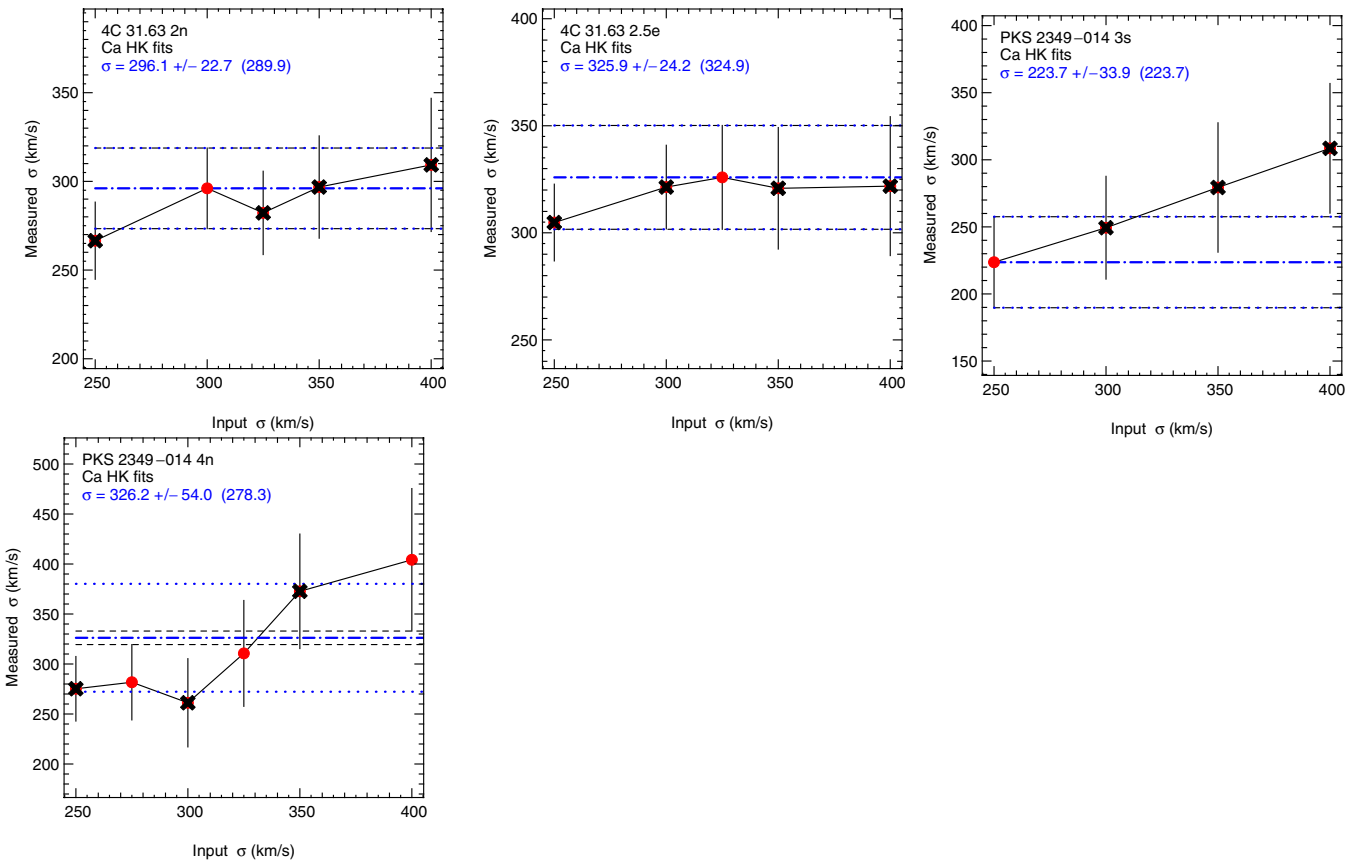

Figure 13. (Continued)

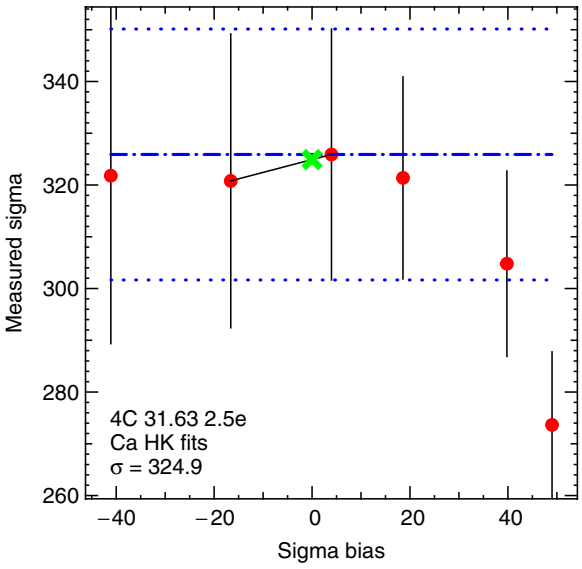

Figure 14. Interpolation of measured σ_* to zero bias.
(A color version of this figure is available in the online journal.)

In all cases, we are left with 1–3 points that have a relatively low sigma bias in the measurement. If we plot the measured σ_* versus σ-bias, as shown in Figure 14 for 4C 31.63 2.5E, we can interpolate between σ-bias values to obtain a measured σ_* that has zero σ-bias (marked by a green cross). Velocity dispersions obtained in this manner are shown in parentheses on the plots in Figure 13 and represent our adopted σ_* values for all galaxies except PG 0052+251. In this case, all measurements within our data resolution ($\sigma_{\rm input} > 250$ km s^{-1}) were sigma biased. From the behavior of the measurements, it appears that the σ_* value with a zero sigma bias falls well below our measurement resolution. Therefore, we can only set an upper limit of $\sigma_* < 250$ km s^{-1} for this galaxy.

The black dashed lines in the plots mark the error bar overlap region of the unbiased measurements and the blue dash-dotted line marks the center of this region. We adopt the average uncertainty of all good measurements (marked by the blue dotted lines).

One last concern is the possibility of galaxy absorption line dilution by residual scattered quasar light inflating the measured velocity dispersion. Since many of the host galaxies with Keck data have measured velocity dispersions near the instrumental resolution, we wished to test whether a lower σ actually could be measured in the presence of line dilution. We tested this effect via simulations in which we generated a model spectrum from Bruzual & Charlot (2003) for a 5 Gyr old galaxy with [Fe/H] = 0.0, smoothed it to $\sigma = 200$ km s^{-1}, added Gaussian noise to achieve S/N = 5 Å^{-1}, and added varying fractions of quasar light using our observed spectrum of PG 1309+355 (which has an instrument resolution of 110 km s^{-1}). We measured velocity dispersions in the same manner as for the host galaxies for simulated quasar light fractions of 0.1–0.5. The results are shown in Figure 15. The top plot shows measured σ as a function of quasar light fraction. Our results show that up to 50% of the spectrum could be due to residual scattered quasar light without adversely affecting the measurement of velocity dispersion for a galaxy with $\sigma = 200$ km s^{-1}. The bottom two plots show the velocity dispersion fits for quasar light fractions of 0.0 and 0.5. Dilution of the lines is obvious.

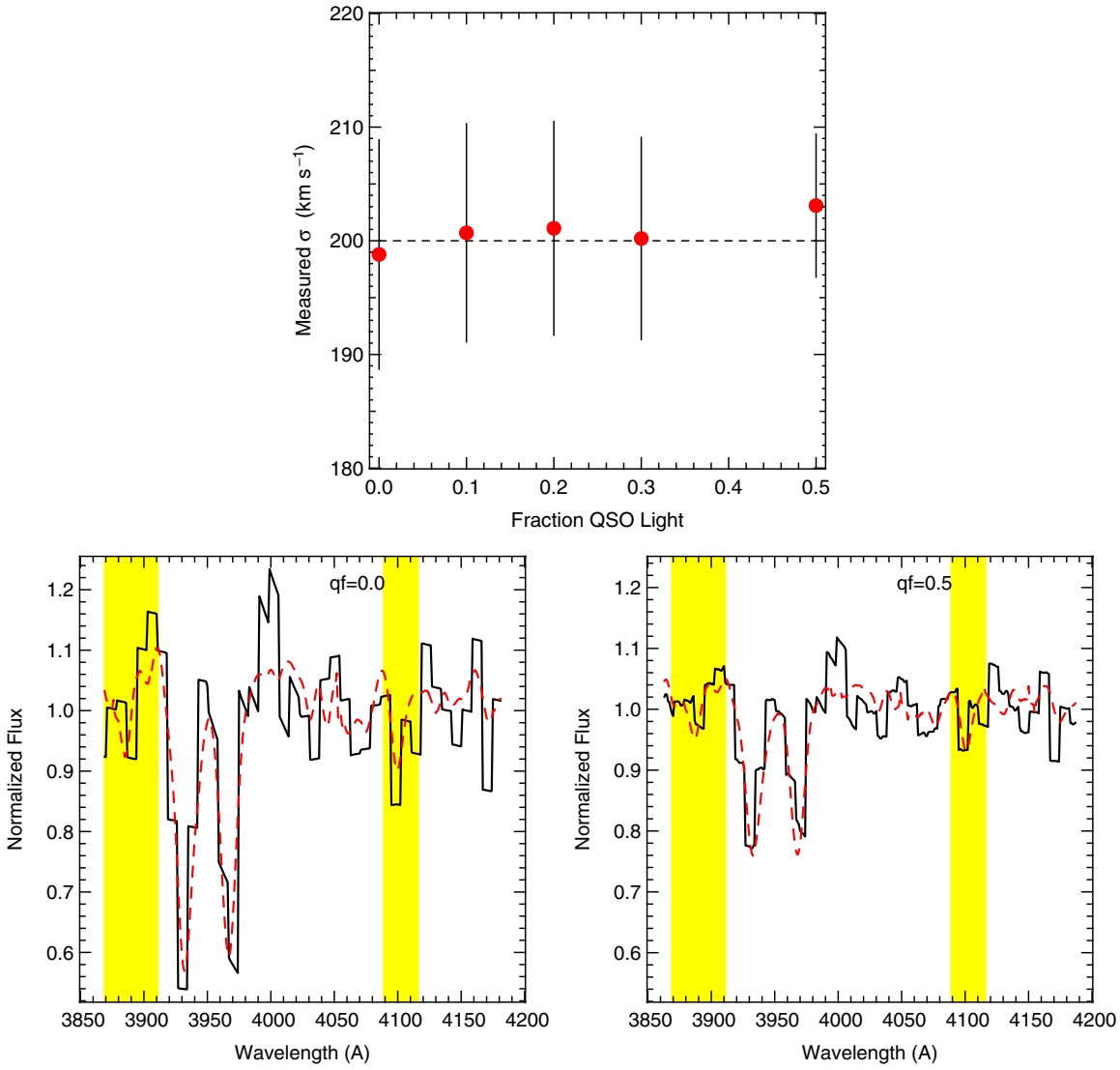

Figure 15. Test of velocity dispersion measurement on galaxy spectra diluted by quasar light. We smoothed a model galaxy spectrum (age 5 Gyr, [Fe/H] = 0.0) to $\sigma = 200$ km s^{-1}, added noise to reach S/N = 5 Å^{-1}, and added different fractions of a quasar spectrum (from PG 1309+355) to dilute the galaxy spectrum. The top plot shows measured σ as a function of quasar light fraction. Up to 50% of the scatter-subtracted spectrum could be residual QSO light without adversely affecting the measurement of velocity dispersion for a galaxy with $\sigma = 200$ km s^{-1}. The bottom plots show the σ fits for quasar fractions of 0.0 and 0.5.

(A color version of this figure is available in the online journal.)

REFERENCES

Bahcall, J. N., Kirhakos, S., Saxe, D. H., & Schneider, D. P. 1997, ApJ, 479, 642
Bahcall, J. N., Kirhakos, S., & Schneider, D. P. 1995, ApJ, 454, L175
Bahcall, J. N., Kirhakos, S., & Schneider, D. P. 1996, ApJ, 457, 557
Baldry, I. K., Glazebrook, K., Brinkmann, J., Ivezić, Z., Lupton, R. H., Nichol, R. C., & Szalay, A. S. 2004, ApJ, 600, 681
Bell, E. F., et al. 2004, ApJ, 608, 752
Bender, R., Burstein, D., & Faber, S. M. 1992, ApJ, 399, 462
Bernardi, M., et al. 2003a, AJ, 125, 1817
Bernardi, M., et al. 2003b, AJ, 125, 1866
Bernardi, M., et al. 2006, AJ, 131, 2018
Bershady, M. A., Andersen, D. R., Harker, J., Ramsey, L. W., & Verheijen, M. A. W. 2004, PASP, 116, 565
Bershady, M. A., Andersen, D. R., Verheijen, M. A. W., Westfall, K. B., Crawford, S. M., & Swaters, R. A. 2005, ApJS, 156, 311
Boroson, T. A., Oke, J. B., & Green, R. F. 1982, ApJ, 263, 32
Boroson, T. A., Persson, S. E., & Oke, J. B. 1985, ApJ, 293, 120
Brinkmann, W., Yuan, W., & Siebert, J. 1997, A&A, 319, 413
Bruzual, G., & Charlot, S. 2003, MNRAS, 344, 1000
Canalizo, G., & Stockton, A. 2000, ApJ, 528, 201
Canalizo, G., & Stockton, A. 2001, ApJ, 555, 719
Cattaneo, A., Dekel, A., Devriendt, J., Guiderdoni, B., & Blaizot, J. 2006, MNRAS, 370, 1651
Cid Fernandes, R., Mateus, A., Sodré, L., Stasińska, G., & Gomes, J. M. 2005, MNRAS, 358, 363
Cimatti, A., et al. 2002, A&A, 381, L68
Coleman, G. D., Wu, C.-C., & Weedman, D. W. 1980, ApJS, 43, 393
Dasyra, K. M., et al. 2006, ApJ, 651, 852
Dasyra, K. M., et al. 2007, ApJ, 657, 102
Dekel, A., & Birnboim, Y. 2006, MNRAS, 368, 2
de Vaucouleurs, G., & Pence, W. D. 1978, AJ, 83, 1163
Drory, N., Feulner, G., Bender, R., Botzler, C. S., Hopp, U., Maraston, C., Mendes de Oliveira, C., & Snigula, J. 2001, MNRAS, 325, 550
Dunlop, J. S., McLure, R. J., Kukula, M. J., Baum, S. A., O'Dea, C. P., & Hughes, D. H. 2003, MNRAS, 340, 1095
Dunlop, J. S., Taylor, G. L., Hughes, D. H., & Robson, E. I. 1993, MNRAS, 264, 455
Faber, S. M., Wegner, G., Burstein, D., Davies, R. L., Dressler, A., Lynden-Bell, D., & Terlevich, R. J. 1989, ApJS, 69, 763
Faber, S. M., et al. 2007, ApJ, 665, 265
Ferrarese, L., & Merritt, D. 2000, ApJ, 539, L9
Franceschini, A., Vercellone, S., & Fabian, A. C. 1998, MNRAS, 297, 817
Fukugita, M., Shimasaku, K., & Ichikawa, T. 1995, PASP, 107, 945
Gebhardt, K., et al. 2000a, ApJ, 539, L13

Gebhardt, K., et al. 2000b, AJ, 119, 1157
Gebhardt, K., et al. 2003, ApJ, 597, 239
Gehren, T., Fried, J., Wehinger, P. A., & Wyckoff, S. 1984, ApJ, 278, 11
Genzel, R., Tacconi, L. J., Rigopoulou, D., Lutz, D., & Tecza, M. 2001, ApJ, 563, 527
Giavalisco, M., et al. 2004, ApJ, 600, L93
Gower, A. C., & Hutchings, J. B. 1984, AJ, 89, 1658
Greene, J. E., & Ho, L. C. 2006, ApJ, 641, 117
Guyon, O., Sanders, D. B., & Stockton, A. 2006, ApJS, 166, 89
Hamilton, T. S., Casertano, S., & Turnshek, D. A. 2002, ApJ, 576, 61
Heavens, A., Panter, B., Jimenez, R., & Dunlop, J. 2004, Nature, 428, 625
Hewitt, A., & Burbidge, G. 1993, ApJS, 87, 451
Ho, L. C. 2002, ApJ, 564, 120
Ho, L. C. 2005, ApJ, 629, 680
Hogg, D. W., et al. 2003, ApJ, 585, L5
Hughes, D. H., Kukula, M. J., Dunlop, J. S., & Boroson, T. 2000, MNRAS, 316, 204
Hutchings, J. B., Janson, T., & Neff, S. G. 1989, ApJ, 342, 660
Hutchings, J. B., & Neff, S. G. 1992, AJ, 104, 1
Jørgensen, I., Franx, M., & Kjærgaard, P. 1995, MNRAS, 276, 1341
Jørgensen, I., Franx, M., & Kjærgaard, P. 1996, MNRAS, 280, 167
Kauffmann, G., et al. 2003a, MNRAS, 341, 33
Kauffmann, G., et al. 2003b, MNRAS, 341, 54
Kellermann, K. I., Sramek, R. A., Schmidt, M., Green, R. F., & Shaffer, D. B. 1994, AJ, 108, 1163
Kobulnicky, H. A., & Gebhardt, K. 2000, AJ, 119, 1608
Koo, D. 2003, in Galaxy Evolution: Theory & Observations, ed. V. Avila Reese, C. Firmani, C. S. Frenk, & C. Allen, RevMexAA (Serie de Conferencias), Vol. 17, 245–246
Koo, D., et al. 2005, in Proc. ESO, Workshop on Multiwavelength Mapping of Galaxy Formation and Evolution, ed. A. Renzini, & R. Bender (Berlin: Springer), 216
Kormendy, J. 2004, in Carnegie Observatories Centennial Symp., ed. L. C. Ho (Cambridge: Cambridge Univ. Press), 1
Labbé, I., et al. 2003, AJ, 125, 1107
Lacy, M. 2006, Astrophysics Update 2 (Germany: Springer Verlag), 195
Lacy, M., Laurent-Muehleisen, S. A., Ridgway, S. E., Becker, R. H., & White, R. L. 2001, ApJ, 551, L17
Laor, A. 2000, ApJ, 543, L111
Liu, C. T., Hooper, E. J., O'Neil, K., Thompson, D., Wolf, M., & Lisker, T. 2007, ApJ, 658, 249
Malkan, M. A. 1984, ApJ, 287, 555
McCarthy, P. J., et al. 2004, ApJ, 614, 9
McElroy, D. B. 1995, ApJS, 100, 105
McLeod, K. K., & Rieke, G. H. 1994, ApJ, 420, 58
McLure, R. J., & Jarvis, M. J. 2004, MNRAS, 353, L45
McLure, R. J., Kukula, M. J., Dunlop, J. S., Baum, S. A., O'Dea, C. P., & Hughes, D. H. 1999, MNRAS, 308, 377
McQuade, K., Calzetti, D., & Kinney, A. L. 1995, ApJS, 97, 331
Miller, J. S. 1981, PASP, 93, 681
Miller, J. S., & Sheinis, A. I. 2003, ApJ, 588, L9
Miller, J., Tran, H., & Sheinis, A. 1996, BAAS, 28, 1301
Nelson, C. H. 2000, ApJ, 544, L91
Nelson, C. H., & Whittle, M. 1996, ApJ, 465, 96
Nolan, L. A., Dunlop, J. S., Kukula, M. J., Hughes, D. H., Boroson, T., & Jimenez, R. 2001, MNRAS, 323, 308
Oke, J. B., et al. 1994, in Proc. SPIE 2198, Instrumentation in Astronomy VIII, ed. D. L. Crawford, & E. R. Craine (Bellingham, WA: SPIE), 178
Poggianti, B. M. 1997, ApJS, 122, 399
Romnev, J., et al. 1984, A&A, 135, 289
Rothberg, B., & Joseph, R. D. 2006, AJ, 131, 185
Schweizer, F. 1996, AJ, 111, 109
Sheinis, A. I. 2001, BAAS, 33, 917
Sheinis, A. I. 2002, PhD thesis, Univ. California
Snellen, I. A. G., Lehnert, M. D., Bremer, M. N., & Schilizzi, R. T. 2003, MNRAS, 342, 889
Stockton, A., & MacKenty, J. W. 1987, ApJ, 316, 584
Storchi-Bergmann, T., Kinney, A. L., & Challis, P. 1995, ApJS, 98, 103
Tacconi, L. J., Genzel, R., Lutz, D., Rigopoulou, D., Baker, A. J., Iserlohe, C., & Tecza, M. 2002, ApJ, 580, 73
Tremaine, S., et al. 2002, ApJ, 574, 740
Treu, T., Woo, J.-H., Malkan, M. A., & Blandford, R. D. 2007, ApJ, 667, 117
Valdes, F., Gupta, R., Rose, J. A., Singh, H. P., & Bell, D. J. 2004, ApJS, 152, 251
Véron-Cetty, M. P., & Véron, P. 1991, A Catalogue of Quasars and Active Nuclei (ESO Sci. Rept. No. 10; 5th ed.; Garching: ESO)
Wolf, M. J., Drory, N., Gebhardt, K., & Hill, G. J. 2007, ApJ, 655, 179
Woo, J.-H., Urry, C. M., Lira, P., van der Marel, R. P., & Maza, J. 2004, ApJ, 617, 903
Woo, J.-H., Urry, C. M., van der Marel, R. P., Lira, P., & Maza, J. 2005, ApJ, 631, 762
Yuan, W., Brinkmann, W., Siebert, J., & Voges, W. 1998, A&A, 330, 108